RSC Advances

PAPER

View Article Online
View Journal | View Issue

Cite this: *RSC Adv.*, 2026, **16**, 12682

A chitosan-based thermosensitive hydrogel incorporating propranolol nanoparticles to promote early osseointegration and peri-implant soft-tissue healing

Zhongxi Sun,[ab] Zhiqiang Qi,[ab] Shuang Song,[c] Xuehan Li,[ab] Kangxing Du,[ab] Guowei Wang*[d] and Xiaojing Wang *[ab]

Based on clinical evidence that propranolol enhances bone mineral density, improves early implant stability, and promotes soft-tissue healing, this study investigated whether its local application around dental implants could coordinately promote early osseointegration and gingival tissue repair. To enable localized drug delivery while minimizing systemic adverse effects such as hypotension associated with oral administration, a chitosan-based thermosensitive hydrogel incorporating propranolol-loaded nanospheres was developed and systematically characterized. Cell models related to osseointegration and gingival healing, including MC3T3-E1, Hacats, and HGFs, were used for *in vitro* evaluation, and an SD rat jaw implant model was established *in vivo*. Multiple assays, including CCK-8, live/dead staining, scratch assays, immunofluorescence, Alizarin Red staining, histological staining, immunohistochemistry, and micro-CT, were performed to assess cell proliferation, migration, adhesion, osteogenic differentiation, soft-tissue-related protein expression, and early peri-implant healing. The results demonstrated that the hydrogel exhibited favorable drug-loading capacity and sustained release behavior. It significantly enhanced cellular proliferation, migration, and adhesion and upregulated osteogenic markers (BGLAP, BMP2, RUNX2) and gingival healing-related proteins (LAMA3, ITGB4), thereby accelerating early peri-implant bone formation and gingival repair. This study is the first to apply propranolol to the integrated regeneration of peri-implant hard and soft tissues, establishing a dual sustained-release thermosensitive hydrogel system for localized delivery. The findings provide a novel and effective strategy for improving postoperative peri-implant healing.

Received 5th January 2026
Accepted 29th January 2026

DOI: 10.1039/d6ra00103c

rsc.li/rsc-advances

1 Introduction

The stability and long-term success of dental implants depend on reliable osseointegration with the alveolar bone and firm soft-tissue integration that establishes a durable biological seal.[1–3] With the increasing application of implant-supported prostheses, the incidence of major biological complications, including peri-implant mucositis (PM) and peri-implantitis (PI), continues to rise[4] and frequently results in implant failure. These complications primarily arise from insufficient osseointegration and inadequate soft-tissue sealing around implants. Current clinical strategies aimed at optimizing peri-implant bone and soft-tissue conditions rely mainly on surgical interventions, such as guided bone regeneration (GBR) and connective tissue grafting (CTG). Although these procedures can improve the peri-implant environment, they involve complex operative protocols, considerable surgical trauma, increased risk, potential rejection reactions, and postoperative infection. Moreover, these approaches require substantial patient tolerance and compliance, which limits their applicability in addressing the growing demand for simplified and minimally invasive strategies that promote peri-implant hard- and soft-tissue healing.[5,6]

Recent studies[7–10] indicate that β-adrenergic receptor (β-AR) blockers increase bone mineral density and reduce fracture risk in patients with osteoporosis, highlighting their potential in the management of bone loss. In the context of soft-tissue repair, β-blockers have been recommended for promoting the healing of chronic and burn-related skin wounds,[11,12] thereby offering new perspectives for improving peri-implant hard- and soft-tissue healing. Propranolol (PROP) is a classic nonselective β-AR blocker with potent antihypertensive activity and is widely used as a first-line therapy for hypertension.[13–15] Our previous work

[a]*Department of Oral Implantology, The Affiliated Hospital of Qingdao University, Qingdao 266000, China. E-mail: wangxj_amy@yahoo.com*
[b]*School of Stomatology, Qingdao University, Qingdao 266003, China*
[c]*Key Laboratory of Shaanxi Province for Craniofacial Precision Medicine Research, College of Stomatology, Xi' an Jiaotong University, Xi' an 710004, China*
[d]*Department of Stomatology, No. 971 Hospital of the Chinese Navy, Qingdao 266000, China. E-mail: wanggw_david@yahoo.com*

has shown that it promotes osteoblast proliferation and differentiation and supports early osseointegration. Its applications in osteoporosis and fracture management continue to expand, and PROP is increasingly regarded as a promising agent for bone regeneration.[16] Besides, clinical observations by our research team showed that patients receiving β-blockers exhibited higher bone mineral density and better primary implant stability than untreated individuals. This finding is consistent with a clinical study reporting that hypertensive patients treated with β-blockers exhibit higher bone density than those not receiving such medication. In contrast, individuals without β-blocker therapy demonstrate poorer initial implant stability, whereas β-blocker use is associated with a markedly reduced risk of implant failure.[10] Epidemiological and retrospective clinical studies have also demonstrated a higher success rate of dental implants among patients taking β-blockers compared to non-users.[17] Preliminary experimental studies further demonstrated that low-dose PROP at 1/10 μM L^{-1} promotes osteogenic differentiation of osteoblasts and bone marrow-derived mesenchymal stem cells (MSCs) by suppressing the cAMP/PKA pathway and upregulating downstream osteogenic markers, including BMP2, RUNX2 and BGLAP, providing a solid basis for further investigation.[16]

In soft tissues, the mucosa, epidermis and subcutaneous layers contain abundant sympathetic nerve fibers that maintain microenvironmental homeostasis.[18] However, sympathetic activation has been shown to impair wound healing.[19,20] Following soft-tissue injury, stress stimulates the adrenal medulla and presynaptic neurons to release large amounts of catecholamines, including epinephrine and norepinephrine (NE), which bind to β-AR on cell membranes and delay wound repair. Keratinocytes, fibroblasts and epithelial cells involved in soft-tissue healing also express these receptors.[21,22] β-blockers competitively bind to and inhibit β-ARs, thereby exerting beneficial effects on soft-tissue repair.[23–25] Preliminary work by our research team demonstrated that PROP promotes early spreading, migration, proliferation, and adhesion of human immortalized keratinocytes (Hacats) and human gingival fibroblasts (HGFs) and enhances the expression of hemidesmosome-related proteins, such as LAMA3 and integrin β4, suggesting its potential to improve peri-implant soft-tissue sealing.[26] Additional *in vitro* and *in vivo* studies have further shown that PROP, as a nonselective β-blocker, improves healing in acute and chronic refractory wounds, severe burns, ulcerative infantile hemangioma (UIH), corneal injury, and other soft-tissue conditions. Both topical and systemic administration of nonselective β-blockers has been associated with enhanced wound repair.[27–29] Collectively, these findings indicate that β-AR blockers represent a promising adjunctive strategy for soft-tissue wound healing.

However, PROP is primarily administered orally, which requires strict dose control and is associated with adverse effects such as hypotension and bradycardia; prolonged use may also lead to drug tolerance.[30,31] To address these limitations, this study investigated the local delivery of PROP to the implant site to enhance peri-implant hard- and soft-tissue healing while minimizing systemic complications. Drug-loaded hydrogels provide a feasible approach to achieving this objective. Thermosensitive hydrogels are injectable,[32] enable efficient delivery to defect sites, maintain local drug concentrations, and reduce dosing frequency.[33] However, their application in drug-release systems remains limited.[34,35] A prolonged

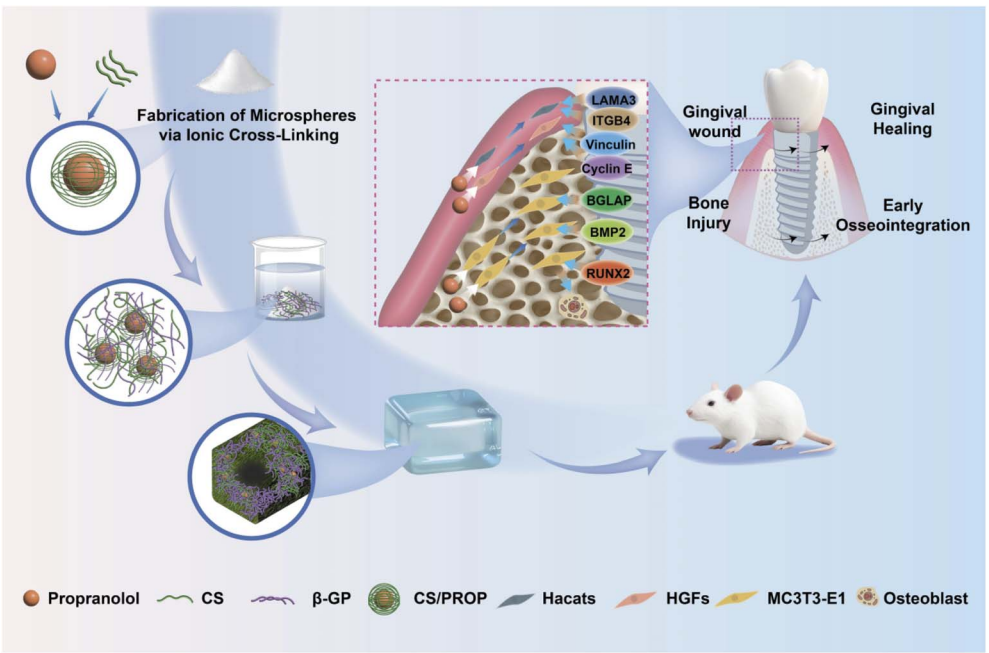

Scheme 1 Preparation of the thermosensitive CS-PROP nanosphere hydrogel and its role in accelerating gingival healing and early osseointegration. The hydrogel enhances the proliferation, migration, and adhesion fibroblasts and epithelial cells, increases the expression of key healing-related proteins, and promotes osteoblast proliferation and osteogenic differentiation.

response time is considered a major drawback, and instability in rheological behavior represents an additional challenge.[36] Therefore, the effective application of stimulus-responsive hydrogels in drug-delivery systems depends on achieving controlled release while maintaining material stability. Chitosan (CS) has been widely used in the preparation of sustained-release microspheres and temperature-responsive drug-loaded hydrogels[37,38] and is regarded as a highly promising carrier for drug-delivery systems,[39] as it supports stable and gradual release of bioactive factors.[40] In the present study, PROP-loaded CS nanospheres were fabricated using an ionic crosslinking method. Nanosphere-mediated controlled release was employed to protect PROP and regulate its sustained delivery, and the nanospheres were subsequently incorporated into a CS-β-glycerophosphate (GP) hydrogel to achieve a dual-stage release profile, resulting in a thermosensitive CS/PROP nanosphere hydrogel (Scheme 1).

The influence of PROP on peri-implant bone and gingival healing within the oral environment remains incompletely understood. Therefore, this study examined whether the β-AR blocker PROP promotes coordinated soft- and hard-tissue regeneration around dental implants. The effects of the hydrogel on cells involved in peri-implant healing, including MC3T3-E1 cells, Hacats and HGFs, were evaluated. In addition, a mandibular implant model in Sprague–Dawley (SD) rats was established to further assess peri-implant bone formation and gingival healing following local drug administration. The feasibility of localized PROP delivery using a dual-release hydrogel system was also investigated, providing new insights into its potential clinical translation.

2 Results and discussion

2.1 Characterization of the CS/PROP/CS-GP hydrogel

CS is one of the most abundant natural polysaccharides and is widely used in regenerative medicine and tissue engineering. Its potential as a drug carrier has attracted considerable interest.[41] In the present study, the CS-GP hydrogel appeared transparent, whereas incorporation of CS/PROP nanospheres resulted in an opaque, milky-white formulation (Fig. 1a). CS exhibits several favorable pharmacological properties, including adhesion, biodegradability, osteogenic activity, and transient modulation of epithelial tight junctions.[41] These characteristics support its application as a delivery system for oral,[42] ocular, intestinal,

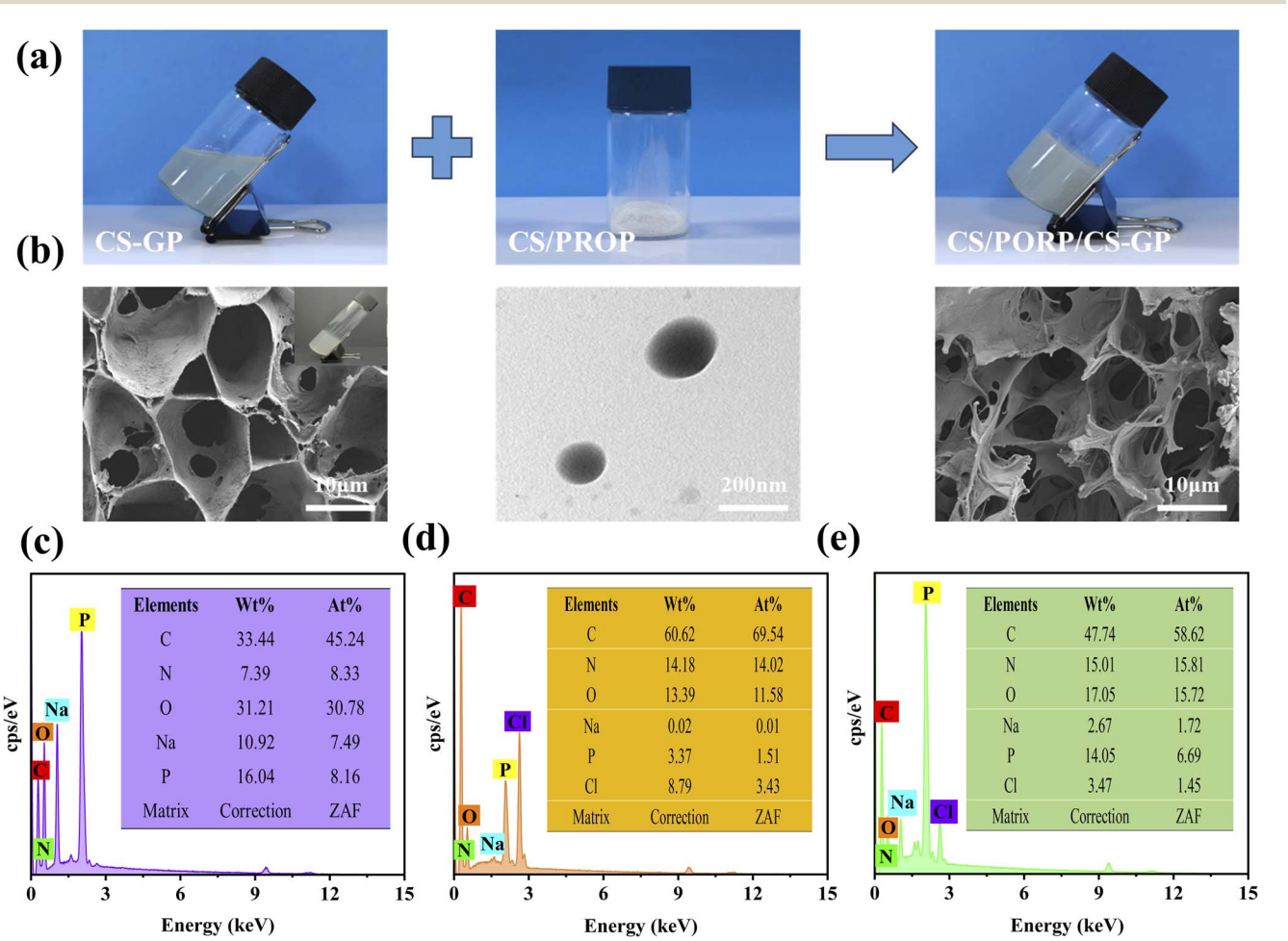

Fig. 1 Photographs of the hydrogel before and after gelation and characterization of its physicochemical properties. (a) Preparation of the CS/PROP/CS-GP hydrogel. (b) SEM images of CS-GP and CS/PROP/CS-GP hydrogels and a TEM image of CS/PROP nanospheres. (c–e) EDS spectra of the CS-GP hydrogel, CS/PROP nanospheres, and CS/PROP/CS-GP hydrogel.

pulmonary, and nasal administration. Owing to these advantages, CS is commonly employed as a base material for nanospheres to achieve efficient drug delivery and sustained release.[43] SEM images revealed a relatively uniform porous structure capable of providing structural support for the CS/PROP nanospheres. TEM further confirmed that the nanospheres were spherical with smooth surfaces and a uniform size distribution (Fig. 1b), with an average diameter of 305.51 ± 5.5 nm. The encapsulation efficiency of CS/PROP was 63.84 ± 1.60%, and the drug-loading capacity reached 61.37 ± 2.71%.

EDS analysis showed that the CS/PROP/CS-GP hydrogel contained characteristic elements derived from both CS-GP and CS/PROP (Fig. 1c–e). The C/Cl ratio of CS/PROP was 20.247, whereas that of the CS/PROP/CS-GP hydrogel increased to 40.427. Similarly, the C/O ratio of CS-GP was 1.469, which was lower than that of the CS/PROP/CS-GP hydrogel (3.729). These changes in elemental composition provide preliminary evidence for successful hydrogel formation. XRD analysis further confirmed structural modification after incorporation. PROP exhibited characteristic diffraction peaks at 2θ = 6.2°, 12.4°, 15.2°, 16.4°, 18.6°, 19.8°, 21.2°, and 23.2°, whereas CS-GP displayed peaks at 2θ = 6.5°, 10.5°, 13.0°, 16.0°, 19.5°, 21.5°, 23.5°, 26.5°, and 29.5°. In contrast, the CS/PROP/CS-GP hydrogel showed distinct diffraction peaks at 2θ = 11.01°, 12.58°, 16.77°, 17.26°, 25.14°, and 29.86° (Fig. 2a). The shift in peak positions indicates that the structural characteristics of CS/PROP were altered after encapsulation within the CS-GP matrix, leading to the formation of a new phase. FTIR spectra of CS-GP, CS/PROP, and CS/PROP/CS-GP are presented in Fig. 2b. For CS, O–H stretching appeared at 3389 cm^{-1} and –NH_2 stretching was observed at 1578 cm^{-1}. CS/PROP exhibited O–H stretching at 3281 cm^{-1}, N–H stretching at 2968 cm^{-1}, C–O–C stretching at 1106 cm^{-1}, aromatic C=C stretching at 1587 cm^{-1}, and a characteristic α-substituted naphthalene peak at 797 cm^{-1}.[44] The CS/PROP/CS-GP hydrogel retained all characteristic absorption peaks of both CS-GP and CS/PROP, confirming the successful integration of the two components and the formation of the composite hydrogel.

Hydrogels function as drug-delivery carriers capable of maintaining local drug concentrations through storage, controlled release, and release-driving mechanisms.[45] Appropriate rheological behavior is essential for ensuring their stability within tissues. The storage modulus (G') and loss modulus (G'') are key parameters describing hydrogel viscoelasticity, with G' reflecting the integrity and connectivity of the polymer network. As shown in Fig. 2c, in all groups, G' was initially lower than G''. As temperature increased, G' increased and intersected with G'', indicating the occurrence of a sol–gel transition. Upon reaching 37 °C, G' became significantly higher than G'', demonstrating that all hydrogels maintained their internal network structure and exhibited stable mechanical properties. Previous studies have confirmed that the encapsulation of sustained-release microspheres does not significantly affect gelation time or rheological behavior.[46] According to the results shown in Fig. 2c, the CS/PROP/CS-GP solution began transitioning from sol to gel before reaching 37 °C, which is consistent with the results presented in Fig. 2d. The fundamental driving force behind this phenomenon lies in the fact that an increase in temperature disrupts the electrostatic interactions and hydrogen-bonding networks between chitosan molecular chains and water molecules, as well as within the CS/GP complexes. Concurrently, it enhances hydrophobic interactions and hydrogen-bond crosslinking among polymer chains, thereby leading to the formation of a continuous three-dimensional network with elastic solid-like characteristics throughout the system. At the macroscopic level, this process manifests as a sharp rise in viscosity, resulting in the formation of a non-flowable hydrogel at 37 °C.[47,48] The viscosity-temperature profiles of all hydrogel groups exhibited similar trends without noticeable differences, indicating that the addition of PROP or CS/PROP nanospheres did not adversely affect the rheological performance of the hydrogels (Fig. 2d).

Ultraviolet-visible scanning of the PROP solution over the range of 500–700 nm identified a characteristic absorption peak at 290 nm (Fig. 2e), consistent with previous reports.[49] The standard concentration curve yielded a linear regression equation of $Y = 0.019615X - 0.01416$ ($R^2 = 0.99857$) (Fig. 2f), where Y represents the absorbance at 290 nm and X denotes the PROP concentration. PROP concentrations in the release medium were calculated based on this equation. To prevent premature drug leakage, PROP was first encapsulated in CS nanospheres prior to incorporation into the hydrogel, thereby forming a dual-release system. Degradation assays conducted in SBF (simulated body fluid) and AS (artificial saliva) showed that CS/PROP/CS-GP hydrogels exhibited degradation rates of 57.34 ± 1.16% and 67.62 ± 1.36% at 24 h, respectively (Fig. 2g). Drug-release profiles further demonstrated that CS/PROP/CS-GP hydrogels achieved a more sustained and stable release than PROP/CS-GP hydrogels, whereas the final cumulative release amounts were comparable. On day 10, cumulative release reached 69 ± 3.9% for PROP/CS-GP and 56 ± 2.2% for CS/PROP/CS-GP. By day 30, the cumulative release increased to 80 ± 4.1% and 76 ± 2.1%, respectively (Fig. 2h). These results indicate that incorporation of CS/PROP nanospheres does not impair drug release and supports stable, prolonged pharmacological activity.

2.2 Effects of CS/PROP/CS-GP hydrogel on cells

2.2.1 Screening of PROP concentration. Cell compatibility is a fundamental criterion for evaluating the safety and functional reliability of biomaterials, particularly those intended for long-term contact with internal tissues. High compatibility is essential for maintaining material stability and sustained biological performance.[50] To assess compatibility, three cell types associated with peri-implant soft- and hard-tissue healing, MC3T3-E1, Hacats and HGFs cells, were examined. As shown in Fig. 3a, treatment with PROP at concentrations of 0.1 μM L^{-1} and 1 μM L^{-1} for 36 h significantly enhanced the proliferation of all three cell types ($P < 0.05$). In contrast, exposure to 50 μM L^{-1} PROP reduced cell viability, indicating cytotoxic effects. Based on the CCK-8 results obtained from the three cell types, propranolol at 1 μM L^{-1} exhibited a stronger pro-proliferative trend than the 0.1 μM L^{-1} concentration. In addition, our

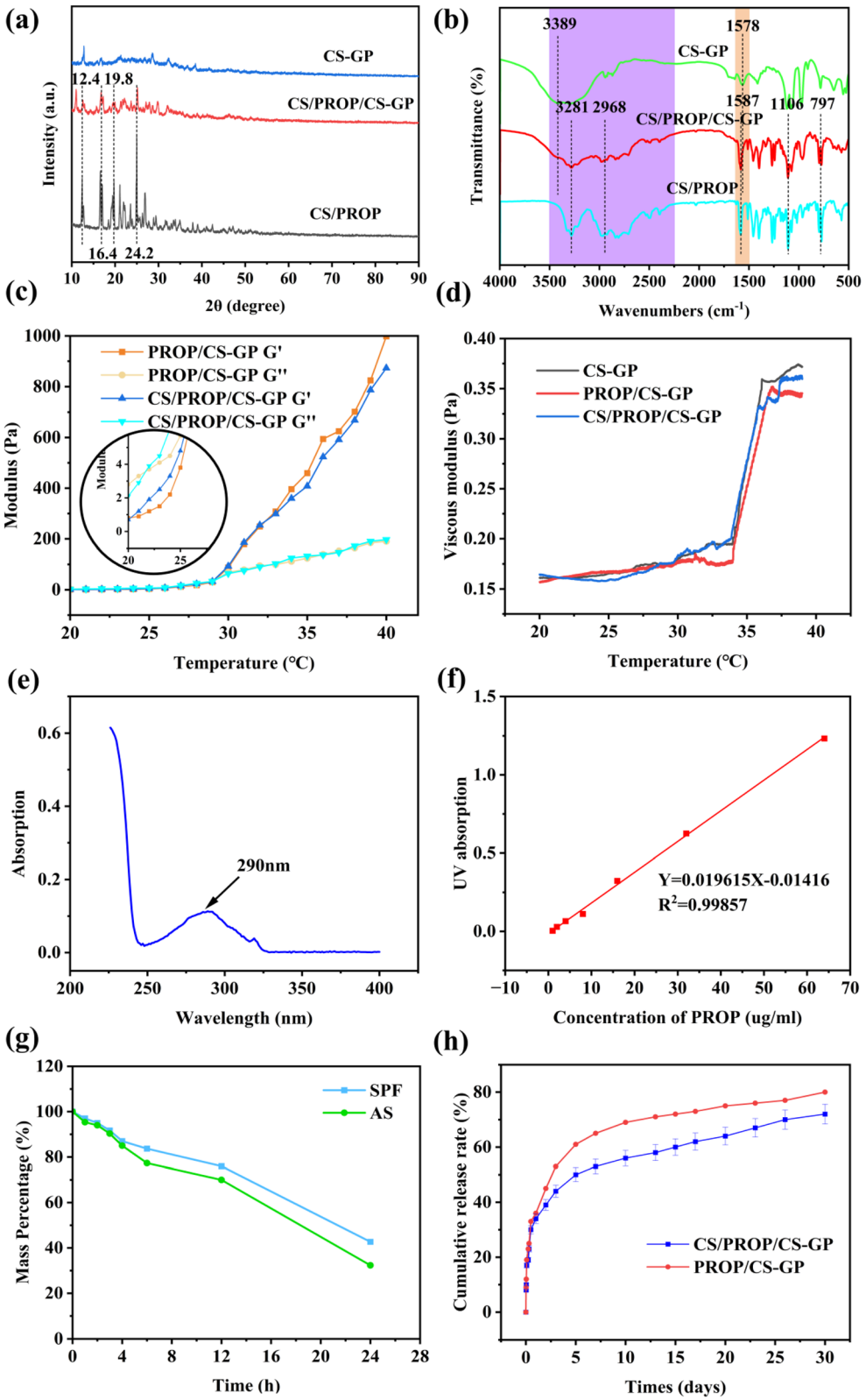

Fig. 2 (a) XRD patterns of CS-GP, CS/PROP, and CS/PROP/CS-GP. (b) FTIR spectra of the three formulations. (c) The temperature-dependent rheological profiles of PROP/CS-GP and CS/PROP/CS-GP hydrogels. (d) Temperature-dependent viscosity during heating (1 °C min^{-1}). (e) Determination of PROP's characteristic absorption wavelength and (f) its standard curve. (g) *In vitro* degradation of CS/PROP/CS-GP hydrogels under simulated physiological conditions (SBF: simulated body fluid; AS: artificial saliva). (h) *In vitro* release profiles of PROP from PROP/CS-GP and CS/PROP/CS-GP hydrogels.

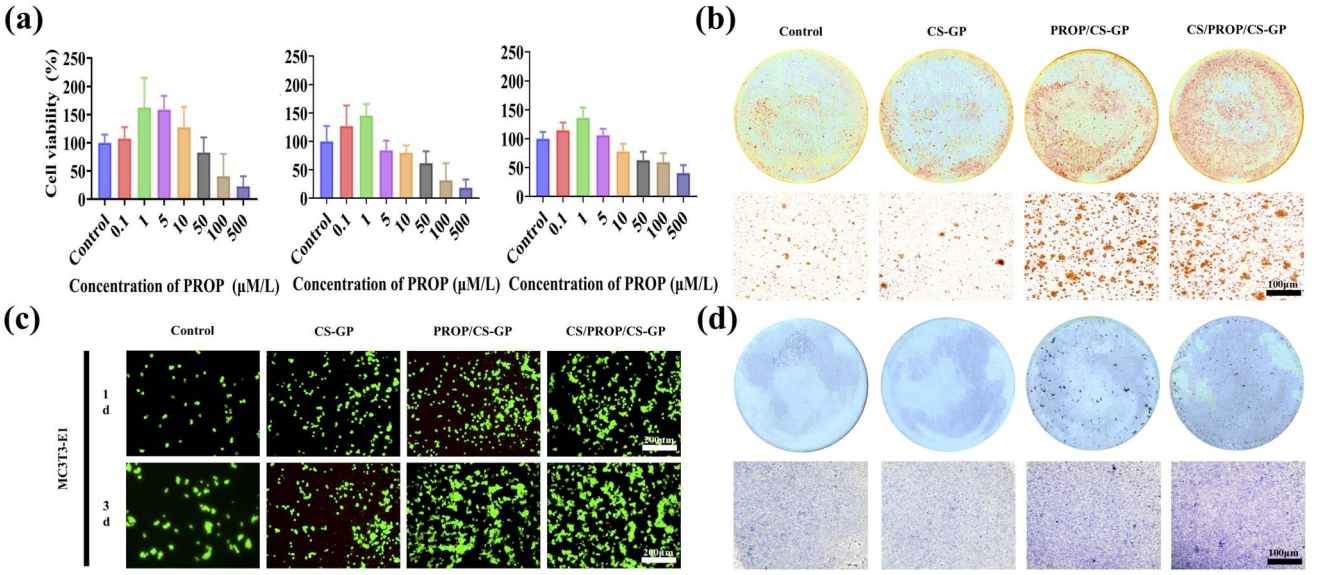

Fig. 3 Screening of the optimal PROP concentration and its effects on MC3T3-E1 cell proliferation and osteogenic differentiation. (A) CCK-8 assay results for MC3T3-E1, Hacats, and HGFs exposed to different PROP concentrations (0.1 μM L^{-1}, 1 μM L^{-1}, 5 μM L^{-1}, 10 μM L^{-1}, 50 μM L^{-1}, 100 μM L^{-1}, 500 μM L^{-1}). (B and D) ALP staining and Alizarin Red staining of MC3T3-E1 cells after 7 and 14 days of osteogenic induction. (C) Fluorescence images of MC3T3-E1 cells stained with FDA/PI.

previous studies[16] have confirmed that 1 μM L^{-1} propranolol exerts superior biological effects compared with 0.1 μM L^{-1}. Taking these findings together with considerations of potential cytotoxicity, a concentration of 1 μM L^{-1} propranolol was ultimately selected for all subsequent experiments.

2.2.2 MC3T3-E1 cells. β-AR blockers, including PROP, have been shown to enhance osteoblast proliferation and differentiation,[51,52] consistent with previous findings from our research team demonstrating increased osteogenic differentiation of osteoblasts and MSCs following β-blocker treatment. In the present study, MC3T3-E1 cells cultured in extracts from PROP/CS-GP and CS/PROP/CS-GP hydrogels exhibited high viability, as evidenced by abundant FDA-positive (green) live cells and very few PI-positive (red) dead cells compared with the control group (Fig. 3c). Alizarin Red staining revealed increased formation of mineralized nodules in both hydrogel groups, with the most pronounced effect observed in the CS/PROP/CS-GP group. ALP staining showed a similar trend. Collectively, these results indicate that CS/PROP/CS-GP hydrogels more effectively promote MC3T3-E1 cell proliferation and osteogenic differentiation (Fig. 3b and d).

2.2.3 Hacats and HGFs cells. PROP is a nonselective β_1- and β_2-adrenergic receptor blocker that was first introduced clinically in 1964 for the treatment of coronary insufficiency[53] and is now widely regarded as a first-line therapy for hypertension and cardiovascular disease.[54–56] Its competitive inhibition of epinephrine and NE at β_1- and β_2-ARs is well established, and numerous studies have demonstrated that PROP suppresses β_2-AR expression.[57,58] During soft-tissue injury, large amounts of epinephrine and NE are released and bind to β-AR on cell membranes, thereby delaying wound repair. Peri-implant soft tissue consists of an epithelial layer and underlying connective tissue, both of which contribute to the formation of a protective biological seal. Epithelial cells, which serve as the primary functional component of the peri-implant epithelial barrier, express β_2-AR.[12,59,60] Implant placement disrupts the native epithelial seal that separates the oral cavity from the submucosa, thereby triggering epithelial proliferation, directional migration, and adhesion to the implant or abutment surface to re-establish the barrier. Fibroblasts, which also express β_2-AR, constitute the connective-tissue component of the peri-implant seal and secrete collagen fibers that provide structural support for the overlying epithelium.[61,62] Together, the epithelial barrier and connective-tissue seal prevent bacterial invasion, protect the underlying bone, and maintain normal gingival architecture.[26]

Accordingly, this study evaluated the effects of the CS/PROP/CS-GP hydrogel on epithelial and fibroblast migration, proliferation, and adhesion, and examined the expression of migration- and adhesion-related proteins to elucidate its influence on cellular behaviors relevant to peri-implant soft-tissue sealing. Hacats and HGFs exhibited high viability in the PROP/CS-GP and CS/PROP/CS-GP extract groups, as indicated by extensive FDA-positive (green) fluorescence and minimal PI-positive (red) fluorescence (Fig. 4a). Early adhesion of epithelial cells and fibroblasts cultured on titanium discs for 6 and 12 h is shown in Fig. 4d. DAPI staining revealed round blue nuclei, and the number of adherent cells increased over time in all groups. SEM images (Fig. 4b) demonstrated initial cell spreading after 12 hours of culture in the different extracts. Cells treated with PROP/CS-GP and CS/PROP/CS-GP exhibited pronounced spreading, with epithelial cells forming dense radiating filopodia or lamellipodia and fibroblasts displaying typical spindle- or star-shaped morphologies with broader spreading areas. In

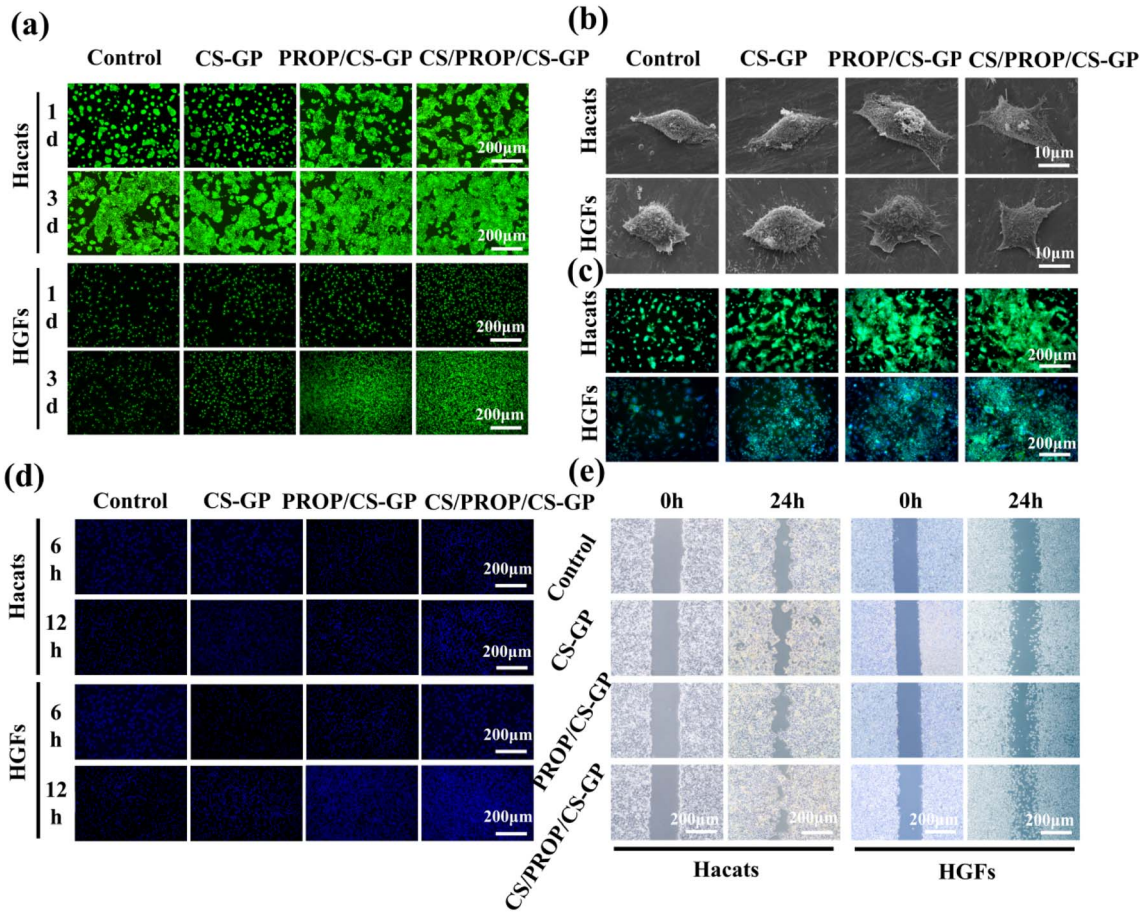

Fig. 4 Effects of the hydrogels on the proliferation, migration, and adhesion of Hacats and HGFs. (a) Fluorescence images of Hacats and HGFs stained with FDA/PI. (b) SEM images showing the morphology of adherent Hacats (top) and HGFs (bottom) on titanium surfaces under different treatment conditions. (c) Immunofluorescence staining of Hacats (top) and HGFs (bottom) cultured on titanium surfaces following different treatments. (d) DAPI staining illustrating early adhesion patterns of Hacats and HGFs on titanium surfaces in each group. (e) Wound-healing assay images of Hacats and HGFs at 0 h and 24 h under each treatment condition.

contrast, cells in the control and CS-GP groups showed only partial spreading with fewer filopodia. Immunofluorescence combined with DAPI staining (Fig. 4c and d) further revealed fewer cells with a more rounded morphology in the control group, whereas cells in the PROP/CS-GP and CS/PROP/CS-GP groups were more numerous and well spread. These findings indicate that both hydrogels enhance Hacats and HGFs spreading and early adhesion on titanium surfaces, with CS/PROP/CS-GP exerting a more pronounced effect, likely attributable to sustained PROP release from the dual-release system. Cell migration is also essential for soft-tissue repair following implantation.[63] Scratch assays performed at 0 and 24 hours showed that CS/PROP/CS-GP markedly enhanced the migratory capacity of Hacats and HGFs (Fig. 4e).

Hemidesmosomes are essential adhesive structures that anchor the junctional epithelium to natural tooth surfaces and the peri-implant epithelium to titanium implants. They are primarily composed of laminin-332, integrin α6β4, and plectin. Laminin-332 is secreted by epithelial cells in response to injury-related signals and binds to integrin α6β4, thereby strengthening epithelial attachment to the titanium surface.[64] Laminin α3 (LAMA3) constitutes the core component of this complex and interacts with integrin receptors to regulate multiple cellular behaviors.[65] Although integrin α6β4 is required for hemidesmosome assembly, the β4 subunit plays a dominant role in coordinating cell–cell and cell–extracellular matrix (ECM) interactions.[66,67] Gingival fibroblasts are the principal cell type within gingival connective tissue and are responsible for collagen synthesis. Adhesion-related proteins, such as vinculin and cyclin E, are critical determinants of fibroblast adhesive capacity and are closely associated with the quality of gingival healing.[68] Accordingly, this study evaluated the expression of LAMA3 and ITGB4 in Hacats and the expression of vinculin and cyclin E in HGFs using immunofluorescence analysis. As shown in Fig. 5a and b, treatment with PROP/CS-GP and CS/PROP/CS-GP hydrogels markedly upregulated the expression of LAMA3, ITGB4, vinculin, and cyclin E compared with the control group, with the CS/PROP/CS-GP hydrogel producing the most pronounced effect. Cells in this group exhibited stronger green and red fluorescence signals within the cytoplasm, whereas the control group displayed the weakest signals and minimal membrane-associated fluorescence. These results indicate that

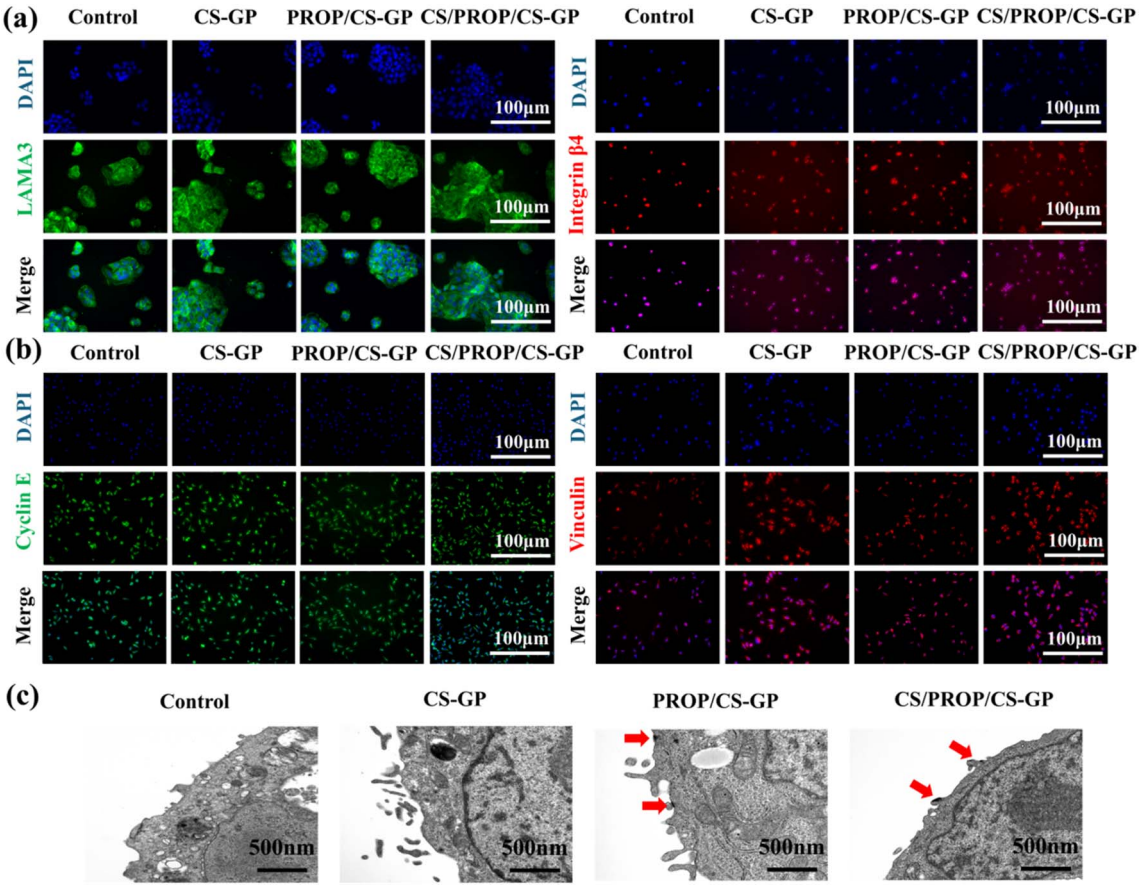

Fig. 5 Effects of the hydrogels on the expression of soft-tissue healing-related protein and hemidesmosome formation in Hacats and HGFs. (a) Immunofluorescence staining of LAMA3 and integrin β4 in Hacats under different treatment conditions. (b) Immunofluorescence staining of cyclin E and vinculin in HGFs following different treatments. (c) Transmission electron microscopy images illustrating hemidesmosome formation in Hacats across treatment groups.

the CS/PROP/CS-GP hydrogel more effectively enhances the expression of LAMA3, ITGB4, vinculin, and cyclin E.

Hemidesmosomes also serve as the principal attachment structures linking epithelial cells to the basement membrane, and analogous structures form at the gingival epithelium–implant interface. Mature hemidesmosomes are well-established indicators of epithelial wound healing in both *in vivo* and *in vitro* studies,[69] and their reformation along the implant surface is essential for establishing a stable epithelial–titanium biological seal during peri-implant epithelial regeneration. After 3 days of Hacats culture, transmission electron microscopy was employed to examine hemidesmosome formation at the cell–titanium interface (Fig. 5c). Hemidesmosomes appeared as electron-dense plaques with high contrast along the cell membrane. In the CS/PROP/CS-GP hydrogel group, cells developed numerous well-defined hemidesmosomes exhibiting the characteristic inverted triangular morphology (red arrows), with the apex oriented toward the intracellular region. Both the number and maturity of these structures were markedly greater than those observed in the other groups. In the PROP/CS-GP group, the electron-dense structures appeared primarily as linear dark plaques rather than classic triangular profiles, suggesting that they may represent hemidesmosome precursors. In contrast, no distinct hemidesmosomal structures were detected in the control group. Collectively, these findings indicate that the CS/PROP/CS-GP hydrogel effectively promotes hemidesmosome formation at the epithelial–implant or abutment interface and thereby accelerates gingival tissue healing. The above results indicate that the CS/PROP/CS-GP hydrogel not only significantly promoted the proliferation and osteogenic differentiation of MC3T3-E1 cells but also markedly enhanced the proliferation, migration, adhesion, and expression of key proteins, including LAMA3, ITGB4, vinculin, and cyclin E, in Hacats and HGFs. These observations are consistent with the mechanism proposed in Scheme 1, in which PROP enhances the biological functions of MC3T3-E1 cells, epithelial cells, and fibroblasts, thereby facilitating early peri-implant osseointegration and soft-tissue healing. Notably, the CS/PROP/CS-GP group exhibited more pronounced osteogenic differentiation (Fig. 2b and d), higher levels of protein expression, and enhanced hemidesmosome formation (Fig. 5), which can be closely attributed to its sustained and stable release of PROP. These *in vitro* findings provide a cellular and molecular basis for the improved early peri-implant osseointegration and accelerated gingival healing observed in subsequent *in vivo* studies and further validate the potential of this dual sustained-

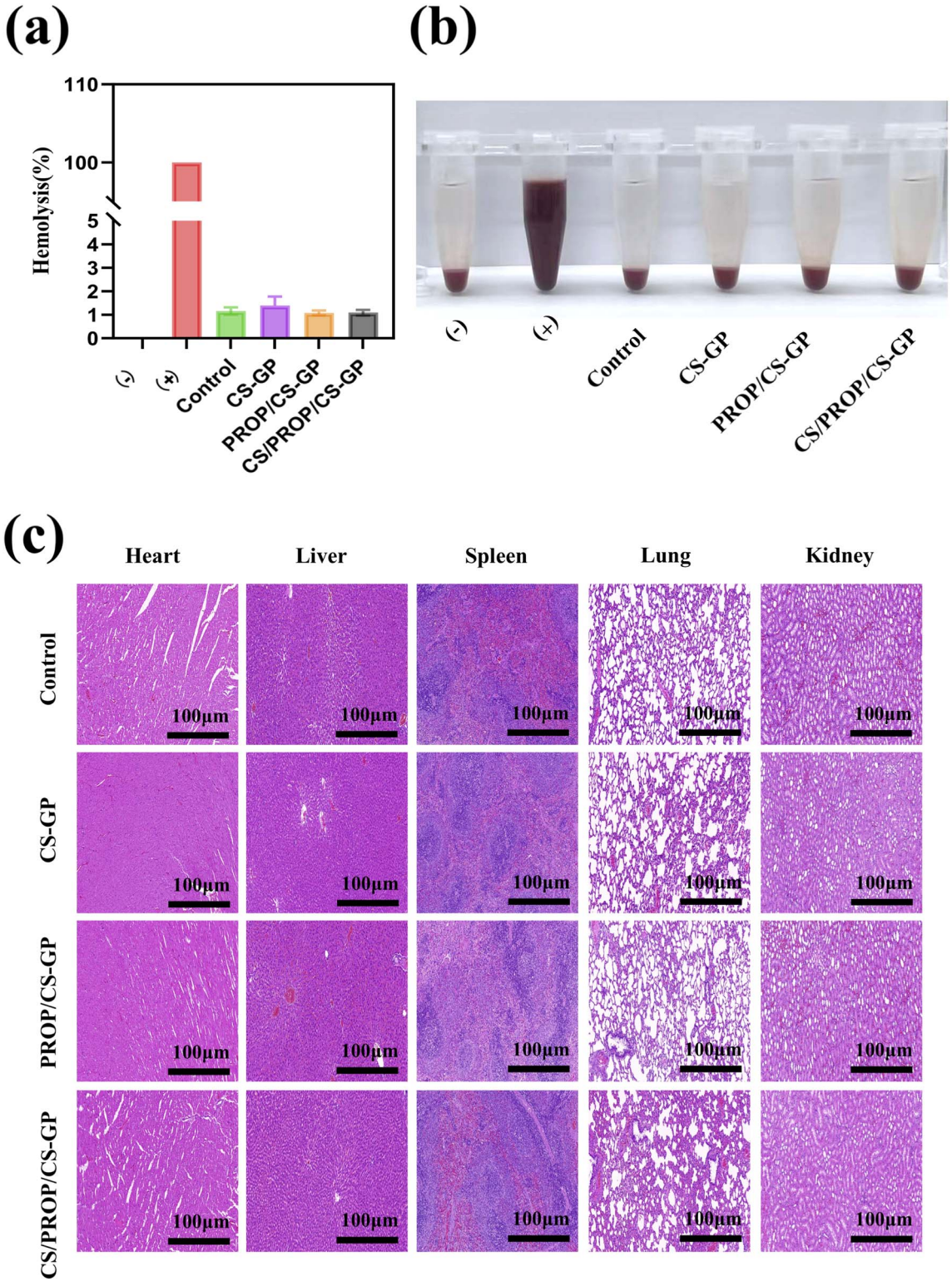

Fig. 6 Hemolysis rates and *in vivo* biosafety evaluation of CS-GP, PROP/CS-GP, and CS/PROP/CS-GP hydrogels. (a and b) Hemolysis assessment using PBS as the negative control (–) and ultrapure water as the positive control (+), together with the hydrogel treatment groups. (c) H&E staining of major organs from rats following administration of each hydrogel formulation.

release system in promoting coordinated peri-implant hard- and soft-tissue regeneration.

2.2.4 Hemocompatibility. Hemocompatibility refers to the ability of a biomaterial to contact blood without eliciting adverse biological reactions. In clinical settings, hemolysis, thrombosis, and immune responses can lead to severe complications.[70] Hemolysis results in red blood cell disruption and may cause anemia and inflammation, thrombosis can

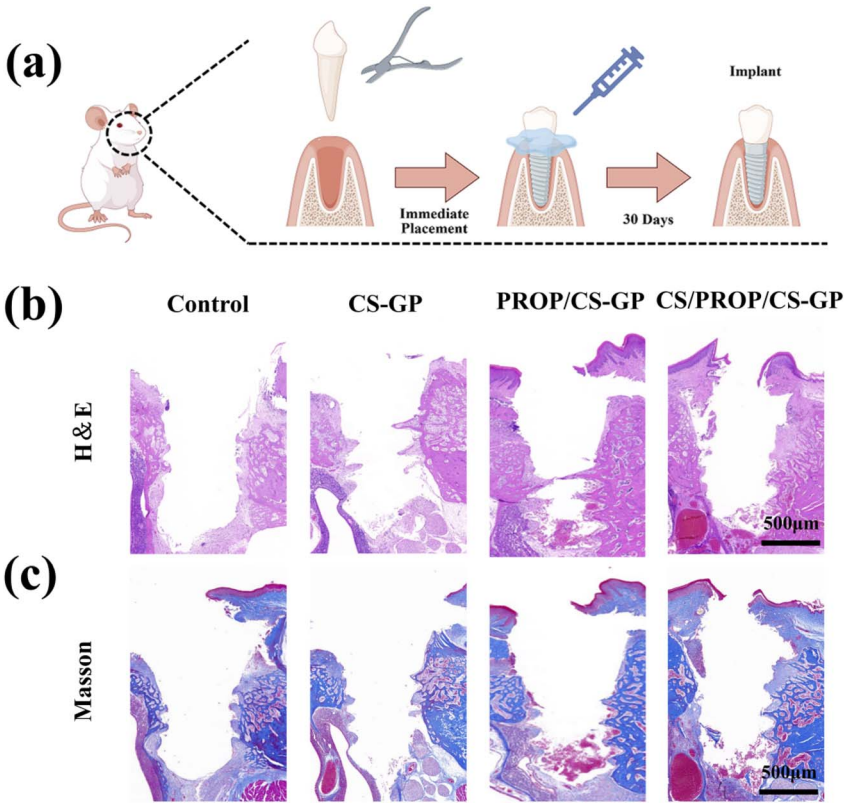

Fig. 7 Effects of CS-GP, PROP/CS-GP, and CS/PROP/CS-GP hydrogels on soft- and hard-tissue healing in an SD rat oral implant model. (a) Schematic illustration of the SD rat implant model. (b) H&E staining of peri-implant maxillary tissues. (c) Masson's trichrome staining of peri-implant maxillary tissues.

obstruct blood vessels, and immune activation may trigger rejection or sepsis. Therefore, materials intended for blood contact are required to exhibit minimal hemolytic and thrombogenic activity while avoiding immune stimulation. To evaluate the hemocompatibility of the CS/PROP/CS-GP hydrogel, a rat blood hemolysis assay was performed, which represents a standard method for assessing erythrocyte rupture following material exposure. Hemolysis is a critical safety indicator, as excessive red blood cell lysis can induce anemia, inflammation, and systemic adverse effects. In this study, the materials were incubated with rat blood under controlled conditions, and hemolysis was quantified by measuring hemoglobin release into the supernatant. Compared with the positive control (100% hemolysis, bright red supernatant) and the negative control (0% hemolysis), all hydrogel groups displayed clear supernatants and significantly lower hemolysis rates below 4% (Fig. 6a and b). These results demonstrate that the CS/PROP/CS-GP hydrogel exhibits excellent anti-hemolytic performance and is suitable for applications involving blood contact. To further assess potential *in vivo* toxicity, major organs of SD rats, including the heart, liver, spleen, lung, and kidney, were examined by HE staining (Fig. 6c). Following treatment with PROP/CS-GP and CS/PROP/CS-GP hydrogels, no pathological abnormalities or adverse tissue responses were observed.

Overall, these findings demonstrate that the drug-loaded hydrogel exhibits excellent cytocompatibility and hemocompatibility and does not induce detectable toxicity in major organs, underscoring its strong potential for biomedical applications.

2.3 Evaluation of the effects of CS/PROP/CS-GP hydrogels on implant placement in rats

The influence of PROP on bone metabolism has been widely documented.[51,71] Minkowitz *et al.*[71] reported enhanced mineral deposition and bone formation in a rat fracture model after nine weeks of PROP treatment, while Bonnet *et al.*[51] demonstrated that low-dose PROP improved bone formation and inhibited osteoclast proliferation in ovariectomized rats. Epidemiological evidence further suggests that β_2-AR blockers may serve as potential therapeutic agents for osteoporosis and fracture management.[72] To avoid systemic adverse effects such as hypotension, CS/PROP nanospheres were prepared in this study using an ionic crosslinking method and subsequently incorporated into a thermosensitive CS hydrogel to generate CS/PROP/CS-GP hydrogels. An SD rat maxillary model was then established to evaluate the *in vivo* efficacy of this formulation (Fig. 7a). HE and Masson staining of peri-implant tissues (Fig. 7b and c) revealed more pronounced regeneration of both bone and gingival tissues in the PROP/CS-GP and CS/PROP/CS-GP groups than in the control group, with the CS/PROP/CS-GP hydrogel producing the most substantial improvement. These findings indicate that the hydrogels enhance peri-implant soft- and hard -tissue healing. Micro-CT analysis based

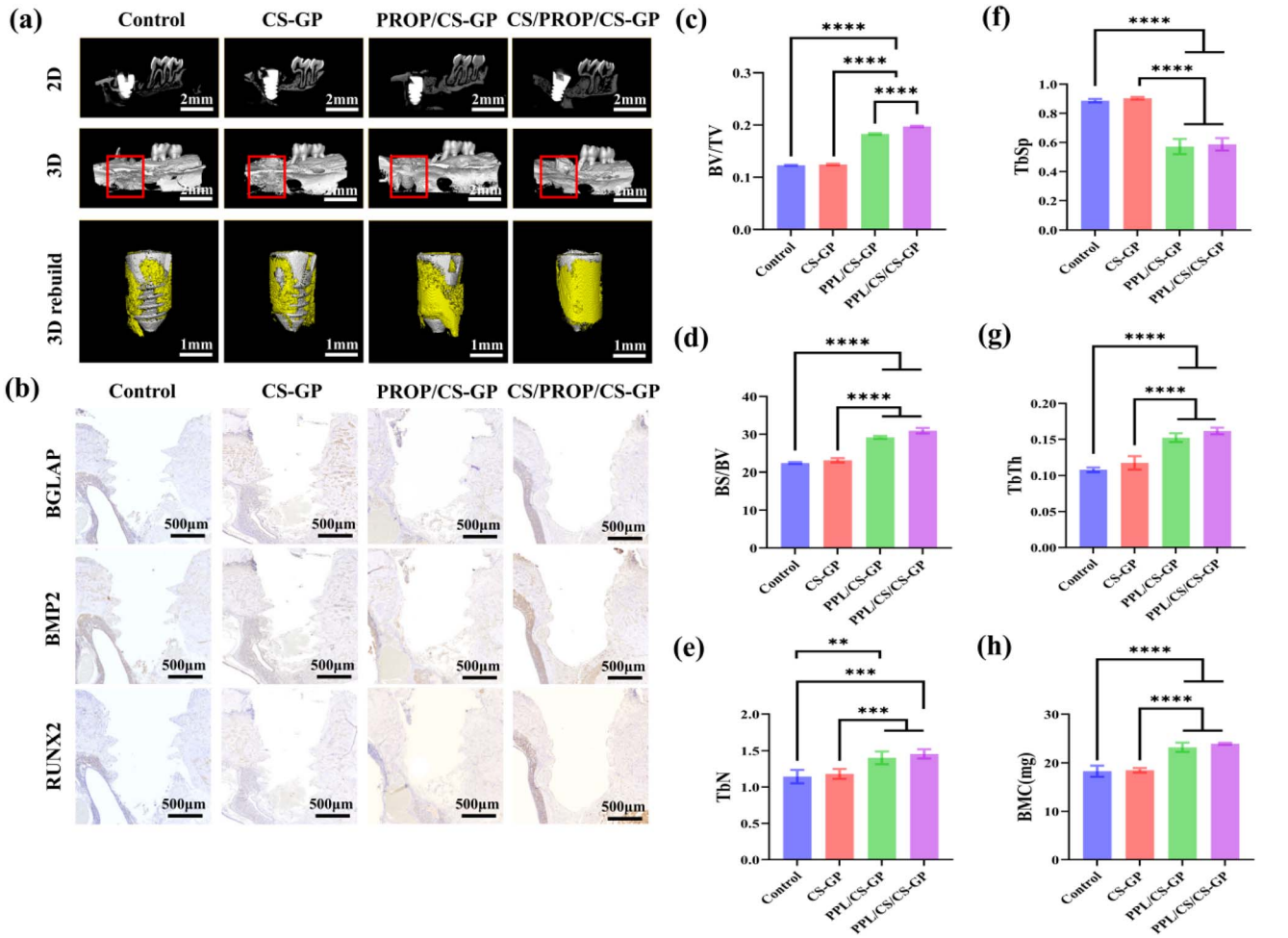

Fig. 8 Effects of CS-GP, PROP/CS-GP, and CS/PROP/CS-GP hydrogels on early peri-implant osseointegration, with micro-CT-based quantitative analysis of newly formed bone. (a) Two-dimensional and three-dimensional micro-CT images of peri-implant maxillary bone and 3D reconstructions of newly formed bone. (b) Immunohistochemical staining of BGLAP, BMP2, and RUNX2 in peri-implant bone. (c) Bone volume (BV)/tissue volume (TV). (d) Bone surface (BS)/bone volume (BV). (e) Trabecular number (Tb.N). (f) Trabecular separation (Tb.Sp). (g) Trabecular thickness (Tb.Th). (h) Bone mineral content (BMC). (**P < 0.01, ***P < 0.001, ****P < 0.0001).

on 2D sections and 3D reconstruction (Fig. 8a) showed that, at 4 weeks after implantation, PROP/CS-GP and CS/PROP/CS-GP hydrogels significantly increased bone volume (BV)/tissue volume (TV) (Fig. 8c), bone surface (BS)/BV (Fig. 8d), trabecular number (Tb.N) (Fig. 8e), trabecular thickness (Tb.Th) (Fig. 8g), and bone mineral content (BMC) (Fig. 8h), while reducing trabecular separation (Tb.Sp) (Fig. 8f). Among the treatment groups, the CS/PROP/CS-GP hydrogel exhibited the most pronounced improvements (P < 0.0001), demonstrating a strong capacity to promote new bone formation around implants. To further confirm its regenerative effects, immunohistochemical analysis was performed to assess the expression of BGLAP, BMP2, and RUNX2 in peri-implant bone, while immunofluorescence staining was used to evaluate integrin β4 and LAMA3 expression in gingival tissues. Osteogenic differentiation is typically accompanied by increased expression of BGLAP, BMP2, and RUNX2.[73,74] In this study, PROP/CS-GP and CS/PROP/CS-GP hydrogels markedly upregulated these osteogenic markers compared with the control group (Fig. 8b), indicating that the hydrogels effectively promote early osteogenesis around the implant.

In soft tissues, immunofluorescence analysis performed at postoperative week 4 showed that LAMA3 was predominantly distributed along the implant–abutment interface and the basal lamina. The PROP/CS-GP and CS/PROP/CS-GP groups exhibited stronger and more extensive LAMA3 fluorescence, suggesting that LAMA3 may guide epithelial healing in the peri-implant region (Fig. 9a). This observation is consistent with previous reports demonstrating that LAMA3 directs epithelial migration during peri-implant epithelial formation.[66] Integrin β4 expression was also higher in the PROP/CS-GP and CS/PROP/CS-GP groups, indicating the presence of hemidesmosomal structures in this region (Fig. 9b). Gürses *et al.*[75] reported that normal junctional epithelium consistently expresses integrin β4, with the internal basal lamina and hemidesmosomes exhibiting characteristic LAMA3 expression. In contrast, the control group displayed weaker and more restricted fluorescence signals for both integrin β4 and LAMA3. Collectively, these findings demonstrate that CS/PROP/CS-GP hydrogels enhance gingival tissue healing and epithelial attachment around implants.

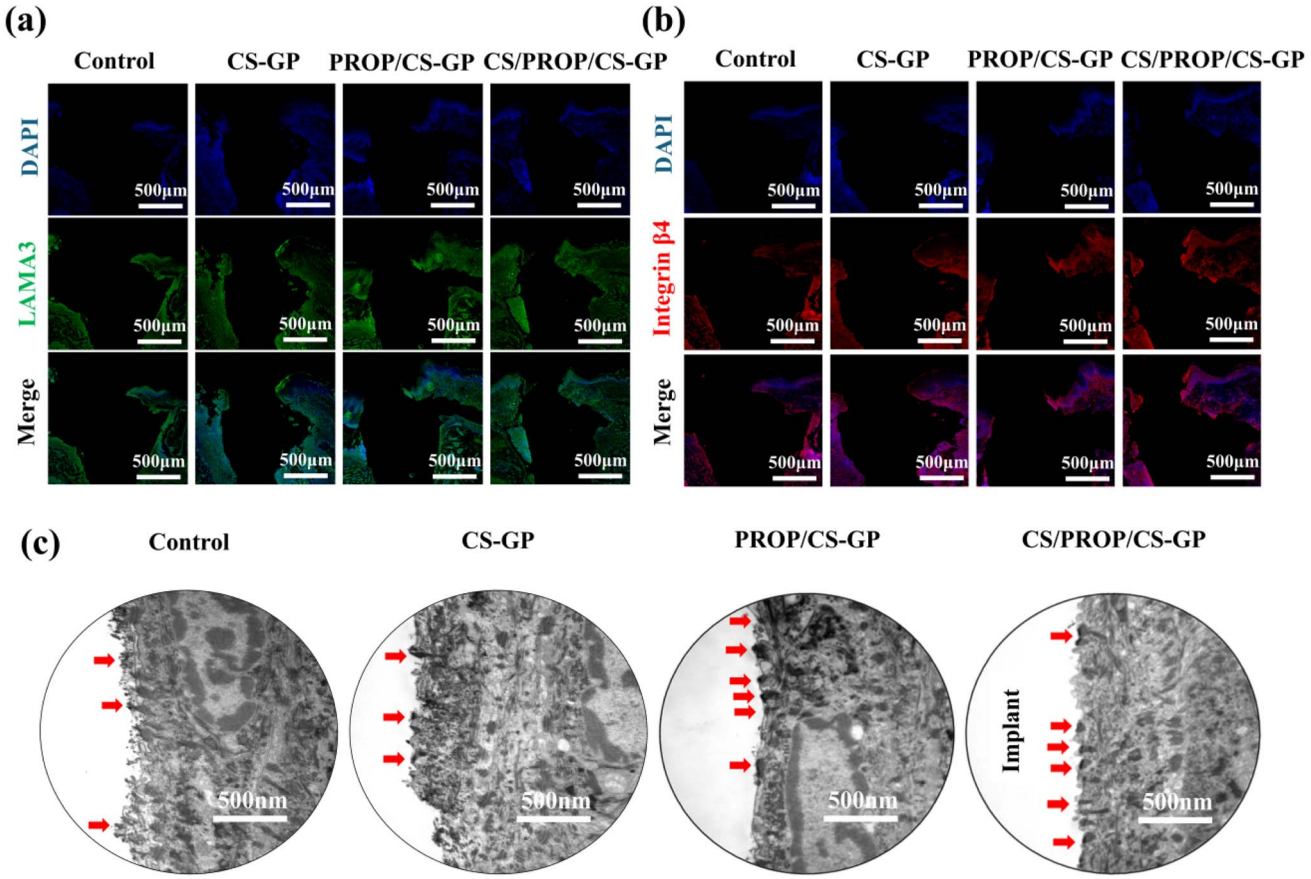

Fig. 9 Effects of CS-GP, PROP/CS-GP, and CS/PROP/CS-GP hydrogels on gingival tissue healing and hemidesmosome formation around implants. (a) Immunofluorescence staining of LAMA3 in peri-implant gingival tissues. (b) Immunofluorescence staining of integrin β4 in peri-implant gingival tissues. (c) TEM images illustrating hemidesmosome formation in peri-implant gingival tissues.

Transmission electron microscopy is a reliable technique for evaluating epithelial attachment at the peri-implant interface. In this study, TEM revealed multiple, relatively continuous hemidesmosomes with well-defined inner plaques at the junction between the junctional epithelium and the implant/abutment surface in the PROP/CS-GP and CS/PROP/CS-GP groups. In contrast, the control group exhibited fewer hemidesmosomes with a more sparse and discontinuous distribution (Fig. 9c). These findings indicate that CS/PROP/CS-GP hydrogels enhance hemidesmosome formation in peri-implant gingival tissues, thereby accelerating soft-tissue sealing and repair. This observation is consistent with previous reports.[76]

In our previous *in vitro* experiments, this study demonstrated that the CS/PROP/CS-GP hydrogel significantly enhances the biological functions of osteogenic and soft-tissue-related cells. To further validate its *in vivo* efficacy, an SD rat implant model was established. Consistent with the *in vitro* findings, the CS/PROP/CS-GP hydrogel markedly promoted peri-implant bone formation (Fig. 8) and gingival tissue healing (Fig. 9). Notably, immunofluorescence analysis revealed significant upregulation of LAMA3 and ITGB4 expression in gingival tissues (Fig. 9a and b), which was in agreement with the enhanced protein expression observed in Hacats cells *in vitro*. In addition, TEM images showed more mature hemidesmosomal structures in the hydrogel-treated group (Fig. 9c), further supporting its role in strengthening the biological seal at the epithelium–implant interface. These *in vivo* results not only corroborate the outcomes of the *in vitro* experiments but also provide further mechanistic insight into how this dual-release system promotes overall peri-implant healing by coordinating hard- and soft-tissue regeneration, as illustrated in Scheme 1.

Moreover, these findings are consistent with recent trends in improving peri-implant healing through localized delivery strategies. For example, functionalized coating materials[1] and growth factor-loaded hydrogels[77] have been shown to effectively enhance osseointegration. Meanwhile, the local application of small-molecule drugs such as β-adrenergic receptor blockers[26] has attracted increasing attention because of their cost-effectiveness and multi-target effects. However, unlike these approaches, which primarily focus on bone repair alone, the present study is the first to demonstrate in a single model that localized delivery of the single agent PROP can synchronously and synergistically enhance both bone and soft-tissue healing. This "two-birds-with-one-stone" strategy offers clear advantages in terms of clinical translational simplicity and cost efficiency compared with more complex systems requiring multiple growth factors.[78]

3 Conclusion

Overall, CS/PROP/CS-GP hydrogels demonstrate strong potential for promoting early osseointegration and gingival soft-tissue healing around dental implants. This dual-release platform integrates CS/PROP nanospheres within a thermosensitive CS-GP hydrogel, and comprehensive physicochemical characterization confirms the successful synthesis of the composite system. Biocompatibility and hemocompatibility evaluations further support its safety. *In vitro*, the hydrogel enhances MC3T3-E1 cell proliferation and osteogenic differentiation and promotes migration, proliferation, adhesion, and related protein expression in Hacats and HGFs. *In vivo*, localized delivery of PROP *via* the drug-loaded hydrogel upregulates osteogenic markers (BGLAP, BMP2, and RUNX2) and gingival healing-related proteins (integrin β4 and LAMA3), thereby accelerating early osseointegration and gingival repair without inducing detectable toxicity in major organs. This study introduces a novel strategy for locally applying the antihypertensive agent PROP to the oral implant microenvironment using a dual-release hydrogel system. Collectively, the *in vitro* and *in vivo* findings demonstrate the substantial potential of this approach to enhance peri-implant soft- and hard-tissue healing and provide a safe and effective platform for postoperative tissue regeneration.

4 Materials and methods

4.1 Preparation of the CS/PROP nanosphere thermosensitive hydrogel

4.1.1 Preparation of CS/PROP nanospheres. CS nanospheres were prepared using an ionic crosslinking method based on the electrostatic interaction between positively charged CS and negatively charged sodium tripolyphosphate (TPP).[79] Briefly, CS powder (0.1 g) was dissolved in 0.1 mol L^{-1} acetic acid, adjusted to a final volume of 100 mL, and magnetically stirred for 1 h to obtain a CS solution with a concentration of 1 mg mL^{-1}. An appropriate volume of the CS solution was then mixed with 5% (w/v) TPP solution added dropwise under continuous stirring until turbidity appeared. Stirring was continued for 30 min, followed by a standing period of 15 min. The supernatant was subsequently collected and ultrasonicated for 5 min to obtain a well-dispersed CS nanosphere suspension. For drug loading, PROP was added to the 1 mg mL^{-1} CS solution to achieve a final concentration of 1 μM L^{-1}. A 5% (w/v) TPP solution was then added dropwise under continuous stirring until turbidity was observed. The mixture was stirred for 30 min and allowed to stand for an additional 15 min. The supernatant was collected and ultrasonicated for 5 min to obtain a uniformly dispersed CS/PROP nanosphere suspension.

4.1.2 Synthesis of CS/β-glycerophosphate (CS-GP) thermosensitive hydrogel. The CS-GP thermosensitive hydrogel was prepared according to a standard protocol.[45] Briefly, CS (0.4 g) was dissolved in 18 mL of 0.1 mol L^{-1} acetic acid, while β-GP (1.12 g) was dissolved in 2 mL of double-distilled water. Both solutions were cooled in an ice bath for 15 min. The β- GP solution was then added dropwise to the CS solution using a 7-gauge syringe under continuous stirring for 15 min. The final concentrations of CS and β-GP were 2% (w/v) and 5.6% (w/v), respectively, and the pH of the mixture was adjusted to 7.15 ± 0.06. The resulting hydrogel precursor solution was stored at 4 °C until use. For drug incorporation, either the CS/PROP nanosphere suspension or a free PROP solution was added to the CS-GP mixture at 4 °C. Each formulation was prepared to a final volume of 20 mL.

4.2 Scanning electron microscopy (SEM)

Freeze-dried CS/PROP/CS-GP hydrogels and CS/PROP powders were sputter-coated with gold, and their surface morphology was examined using SEM and TEM. The particle size distribution of CS/PROP nanospheres was determined using a particle size analyzer.

4.3 FTIR, EDS and XRD analyses

Elemental composition was analyzed using an EDS system. For FTIR analysis, CS-GP, CS/PROP, and CS/PROP/CS-GP samples were each mixed with potassium bromide (KBr) and pressed into pellets, and the characteristic functional groups were recorded over the spectral range of 4000–500 cm^{-1}. XRD analysis of the same samples was performed at room temperature using Cu Kα radiation ($\lambda = 0.154187$ nm). The measurements were conducted at a scanning voltage of 40 kV and a tube current of 40 mA, with a scanning speed of 2° min^{-1}, a step size of 0.02°, and a scan range of 5–90°.

4.4 Rheological measurements

During the measurement using a rotational rheometer (Kinexus Lab+, Malvern Panalytical, UK), the temperature was raised from 20 °C to 40 °C at a constant rate of 1 °C min^{-1}. The variations of storage modulus (G') and loss modulus (G'') with temperature were recorded to evaluate the sol–gel transition process of the hydrogels. Viscosity measurements were performed using a rotational viscometer. Samples were prepared in accordance with the operating requirements of the HAAKE rotational viscometer and measured at a rotational speed of 50 rpm. During the test, the temperature was increased from room temperature to 38 °C at a constant rate of 1 °C min^{-1} to determine the temperature-dependent viscosity of each hydrogel formulation.

4.5 Preparation of the PROP standard curve

Coomassie Brilliant Blue G-250 (CBB G-250) (50.0 mg) was dissolved in 25 mL of 95% ethanol in a 500 mL volumetric flask, followed by the addition of 50 mL of 85% phosphoric acid. The solution was then brought to volume with 0.9% NaCl, filtered, and stored for subsequent use.[47] PROP (1.0 mg) was dissolved in deionized water in a 10 mL volumetric flask to prepare a stock solution with a concentration of 100 μg mL^{-1}. Aliquots of 0.1, 0.2, 0.4, 0.8, 1.6, 3.2, and 6.4 mL of the stock solution were transferred into separate 10 mL test tubes and diluted to volume with deionized water, with deionized water used as the blank control. Subsequently, 5 mL of CBB G-250 solution was added to

each tube and mixed thoroughly. The absorbance was measured at the characteristic wavelength of PROP, and a standard calibration curve was constructed by plotting PROP concentration against absorbance.

4.6 Encapsulation efficiency and drug-loading capacity of CS/PROP

A 0.2 mL aliquot of the supernatant was diluted to a final volume of 1.0 mL with deionized water, followed by the addition of 5 mL of CBB G-250. After thorough mixing, the absorbance was measured at the characteristic wavelength of PROP, and the PROP content in the supernatant was calculated using the standard calibration curve. Encapsulation efficiency and drug-loading capacity were calculated according to the following equations:

$$\text{Encapsulation efficiency (\%)} = (W_1 - W_2)/W_1 \times 100 \quad (1)$$

where W_1 represents the total amount of PROP added, while W2 represents the amount of PROP detected in the supernatant.

$$\text{Drug-loading capacity (\%)} = (W_1 - W_2)/W_3 \times 100 \quad (2)$$

where W1 represents the total amount of PROP added, W2 represents the amount of PROP detected in the supernatant, and W3 represents the mass of CS/PROP nanospheres.

4.7 Hydrogel degradation assay

To simulate physiological conditions, CS/PROP/CS-GP hydrogels were incubated at 37 °C in artificial saliva (AS, Solarbio, China) and simulated body fluid (SBF, G-clone, China). The residual weight of the hydrogels was recorded at 1, 2, 3, 4, 6, 12, and 24 h, with three replicates performed for each group.

For the *in vitro* drug-release study, PROP/CS-GP and CS/PROP/CS-GP hydrogel precursor solutions were incubated at 37 °C to allow gelation, after which the formed gels were transferred into dialysis bags. Each dialysis bag was immersed in a tube containing 50 mL of deionized water and maintained in a shaking water bath at 37 °C (60 rpm, amplitude 24 mm). At predetermined time points, 1 mL of the release medium was collected, and the absorbance was measured using a UV spectrophotometer to determine the PROP concentration. An equal volume of fresh deionized water was added after each sampling to maintain a constant volume. The cumulative release of PROP was calculated using the standard calibration curve according to the following equation: cumulative release (%) = (amount of drug released from the hydrogel/total drug encapsulated in the hydrogel) × 100%.

4.8 Cell and blood compatibility evaluation

4.8.1 PROP concentration screening. Cell proliferation of MC3T3-E1 cells (Procell, Wuhan), Hacats (Shanghai Institute of Biological Sciences, Chinese Academy of Sciences), and HGFs (iCELL Bioscience, China) was evaluated using the Cell Counting Kit-8 (CCK-8) (Meilunbio, Dalian) assay to determine the optimal PROP concentration. After thawing, cells were cultured until adequate spreading was observed and then digested to obtain single-cell suspensions. The cell suspensions were adjusted to a density of 1×10^4 cells mL^{-1}, and 100 μL was seeded into each well of a 96-well plate. Eight experimental groups were prepared and incubated overnight to allow cell attachment. After attachment was confirmed, PROP solutions were added at final concentrations of 0.1, 1.0, 5.0, 10.0, 50, 100, and 500 μM L^{-1} and incubated for 48 h. The cells were then washed with PBS (Pricella, Wuhan), followed by the addition of 100 μL of serum-free DMEM (Pricella, Wuhan) and 10 μL of CCK-8 solution to each well. After incubation for 2 h, absorbance was measured at 450 nm using a microplate reader. The mean optical density (OD) values obtained from replicate wells were used for subsequent statistical analysis.

4.8.2 Cytotoxicity assessment. The cytotoxicity of the hydrogels was evaluated by co-culturing MC3T3-E1 cells, Hacats, and HGFs with hydrogel extracts. Hydrogel samples (100 μL) were immersed in 1 mL of complete DMEM to prepare the extraction solutions. Cells were seeded into 96-well plates at a density of 4000 cells per well and incubated at 37 °C for 24 h. After removal of the original culture medium, the hydrogel extracts were added, and the culture medium was replaced daily. For live/dead staining, cells in each extract group were co-cultured until approximately 80% confluence and then incubated with FDA and PI working solutions (Beyotime, Shanghai, China) in the dark. Cellular morphology and viability in each extract group were subsequently observed using a live-cell imaging system.

4.8.3 Alkaline phosphatase staining. ALP chromogenic staining (Beyotime, Shanghai, China) was used to evaluate early osteogenic activity. MC3T3-E1 cells in good condition were digested with 0.25% trypsin (Pricella, Wuhan), counted, and seeded into 24-well plates at a density of 2×10^4 cells per well. After 24 h of culture, the medium was replaced with osteogenic induction medium, and extraction solutions from the three hydrogel formulations were added to the experimental groups. The culture medium was refreshed every two days. ALP staining was performed on day 7, and the stained cells were observed under an optical microscope at 200× magnification.

4.8.4 Alizarin Red staining. Cell seeding density and culture conditions were identical to those used for ALP staining, with osteogenic induction maintained for 14 days at 37 °C. After induction, mineralized nodule formation was evaluated by Alizarin Red (Oricell, Shanghai, China) staining. Briefly, the culture medium was removed, and the cells were washed three times with PBS, fixed with 4% paraformaldehyde at room temperature for 20 min, and rinsed again with PBS. The cells were then stained with 0.1% Alizarin Red at 37 °C for 30 min, followed by thorough washing with double-distilled water. Stained samples were examined under a light microscope.

4.8.5 Cell spreading and adhesion. Hacats cells (3×10^4 per well) and HGFs cells (2×10^4 per well) were seeded into 24-well plates. The control group was cultured in drug-free medium, whereas the experimental groups were cultured in DMEM containing extracts from the three hydrogel formulations. After 24 h of incubation, non-adherent cells were removed by washing three times with PBS. For SEM analysis, the samples were fixed with

2.5% glutaraldehyde overnight at 4 °C, followed by dehydration, vacuum drying, and sputter coating with gold. Cell morphology on titanium surfaces was then examined by SEM. For immunofluorescence staining, the samples were fixed with 4% paraformaldehyde (Servicebio, China) for 15 min and washed three times with PBS. Cells were permeabilized with Triton X-100 (Solarbio, China) and washed again with PBS. Subsequently, 200 μL of FITC-labeled phalloidin (Solarbio, China) containing 1% bovine serum albumin (Pricella, Wuhan) was added to each well and incubated for 30 min in the dark to label the cytoskeleton. After three additional PBS washes, a ready-to-use DAPI solution (Meilunbio, China) was added and incubated for 3 min to stain the nuclei. Following gentle PBS rinsing on a shaker, the morphology of Hacats and HGFs on titanium surfaces was observed using a fluorescence microscope.

4.8.6 Cell migration. Hacats cells (1×10^4 per well) and HGFs cells (6×10^4 per well) were seeded into six-well plates and cultured to full confluence. Mitomycin C (Pricella, Wuhan) (10 μg mL^{-1}) was added and incubated for 1 h to inhibit cell proliferation. A sterile 10 μL pipette tip was then used to create a straight scratch in each well. Detached cells were removed by gentle rinsing with serum-free DMEM. The control group was cultured in DMEM alone, whereas the experimental groups were supplemented with extracts from the corresponding hydrogel formulations. The plates were incubated for 24 and 48 h. At 0, 24, and 48 h, the samples were washed three times with PBS, fixed, permeabilized, and stained. Cell migration across the scratch area on titanium surfaces was subsequently observed under a microscope.

4.8.7 Immunofluorescence. Immunofluorescence staining was performed to evaluate the expression of hemidesmosome-related proteins, including integrin β4 (ITGB4) (BOSTER, China) and laminin 332 (LAMA3) (BOSTER, China), in Hacats cells, as well as adhesion-related proteins, including vinculin (BOSTER, China) and α-SMA (BOSTER, China), in HGFs cells. Hacats cells (3×10^4 per well) and HGFs cells (2×10^4 per well) were seeded into six-well plates containing 29.7 mm glass coverslips. The control group was cultured in standard medium, whereas the experimental groups were cultured in medium containing extracts from the three hydrogel formulations. After 3 days of culture, the cells were fixed with 4% paraformaldehyde for 15 min and washed three times with PBS on a shaker. The cells were then permeabilized with Triton X-100 for 5 min, followed by three PBS washes and a blocking step for 60 min. Primary antibodies at appropriate dilutions (200 μL per well) were added and incubated overnight at 4 °C. On the following day, the samples were equilibrated to room temperature for 30 min, washed three times with PBS, and incubated in the dark with secondary antibodies diluted 1 : 500 for 1 h. After three additional PBS washes, DAPI was applied for 3 min to stain the nuclei, followed by three final PBS washes. Fluorescence images were acquired using an immunofluorescence microscope.

4.8.8 Transmission electron microscopy for hemidesmosome evaluation. Hacats cells (3×10^4 cells per well) were seeded into 24-well plates and cultured for 3 days in either standard medium or medium containing extracts from the three hydrogel formulations. After removal of the culture medium, the cells were gently rinsed three times with PBS. Cell sheets were detached from the titanium surface using a cell scraper and transferred into 1.5 mL centrifuge tubes with a Pasteur pipette. The samples were centrifuged at 1000 rpm for 3 min to collect cell pellets, washed twice with PBS, and fixed overnight at 4 °C in 2.5% glutaraldehyde (Macklin, China). The cells were subsequently post-fixed in 1% osmium tetroxide for 2 h and washed three times with PBS (15 min each). Dehydration was performed through a graded ethanol series (50%, 70%, 90%, 100%, and 100%; 10 min at each concentration), followed by three dehydration steps in 100% propylene oxide for 30 min each. The samples were then embedded, sectioned, and stained with lead citrate for 10 min, rinsed three times with CO_2-free double-distilled water, and counterstained with uranyl acetate for 30 min, followed by three additional washes. After air drying, ultrathin sections were examined by transmission electron microscopy to evaluate hemidesmosome formation.

4.8.9 Hemolysis assay. Fresh apical blood was collected from healthy rats supplied by Jinan Pengyue Laboratory Animal Breeding Co., Ltd (Jinan, China). Immediately after collection, 500 μL of whole blood was mixed with 5 mL of PBS and centrifuged at 3500 rpm for 5 min. The supernatant was discarded, and the washing procedure was repeated three times. The resulting erythrocyte pellet was resuspended in PBS to obtain a uniform erythrocyte suspension. Aliquots of hydrogel extracts were added to 1 mL of the erythrocyte suspension and incubated at 37 °C for 1 h. After centrifugation, the samples were photographed, and 100 μL of the supernatant was collected to measure the OD at 545 nm using a microplate reader. Ultrapure water and PBS were used as the positive (+) and negative (−) controls, respectively. Hemolysis was calculated according to the following equation:

$$\text{Hemolysis } (\%) = \frac{\text{Abs} - \text{Abs}(-)}{\text{Abs}(+) - \text{Abs}(-)} \times 100\% \quad (3)$$

where Abs represents the absorbance of the hydrogel-treated group, Abs(+) represents the absorbance of the positive control, and Abs(−) represents the absorbance of the negative control.

4.9 Establishment of the rat oral implant model

An oral implant model was established in adult male rats (8 weeks old). After extraction of the left maxillary first molar, a 2 × 2 × 3 mm implant was immediately placed into the extraction socket. The surgical sites were subsequently treated with saline, CS-GP, PROP/CS-GP, or CS/PROP/CS-GP hydrogels. Treatments were administered every 2–3 days for a total duration of four weeks. At the end of the experimental period, the rats were euthanized, and maxillary bone, gingival tissue, and major organs, including the heart, liver, spleen, lung, and kidney, were harvested for further analysis. All surgical and treatment procedures were performed under general anesthesia by the same operator to ensure procedural consistency and minimize inter-operator variability. Excised maxillae were scanned using micro-CT, and ImageJ software was used to quantify peri-implant new bone formation and trabecular microarchitecture. Subsequently, the maxillary specimens were fixed in 4% paraformaldehyde (Servicebio, China) for 48 h and

decalcified in 10% ethylenediaminetetraacetic acid (EDTA) (Solarbio, China) for four weeks. Following decalcification, the tissues were dehydrated, paraffin-embedded, and sectioned parallel to the long axis of the M2 tooth at a thickness of 4 μm. Hematoxylin–eosin (H&E) Masson trichrome staining were performed for histological evaluation. Immunohistochemistry and immunofluorescence staining were used to assess the expression of BGLAP (MCE, China), BMP2 (MCE, China), and RUNX2 (MCE, China) in peri-implant bone tissue, as well as integrin β4 and LAMA3 in peri-implant gingival tissue.

Samples designated for hemidesmosome observation were immediately immersed in pre-cooled glutaraldehyde fixative after harvesting. Following decalcification, the gingival tissue surrounding the implant was carefully dissected. The specimens were trimmed and rinsed three times with PBS for 15 min each, then post-fixed in 1% osmium tetroxide for 2 h and washed three additional times with PBS. Dehydration was performed through a graded ethanol series (50%, 70%, 90%, 100%, and 100%, 10 min at each concentration). The samples were subsequently embedded and sectioned. Ultrathin sections were stained with lead citrate for 10 min and rinsed three times with carbon dioxide-free double-distilled water, followed by staining with uranyl acetate for 30 min and three final rinses with double-distilled water. After air-drying, the sections were examined using a transmission electron microscope. These analyses were used to assess the *in vivo* effects and biosafety of the CS/PROP/CS-GP hydrogel.

4.10 Statistical analysis

All data are presented as the mean ± standard deviation (SD) and were analyzed using GraphPad Prism version 9.5.1. Differences among groups were evaluated by one-way analysis of variance (ANOVA) followed by Tukey's post hoc test. All experiments were performed in triplicate, and error bars represent SD ($n \geq 3$). Statistical significance was defined as $p < 0.05$, with $^{*}p < 0.01$, $^{**}p < 0.001$, and $^{***}p < 0.0001$ indicating increasing levels of significance.

Author contributions

Writing – review & editing, writing – original draft, formal analysis, data curation, Zhongxi Sun; writing – review & editing, formal analysis, data curation, Zhiqiang Qi; writing – review & editing, formal analysis, data curation, Shuang Song; writing – review & editing, formal analysis, data curation, Xuehan Li; writing – review & editing, formal analysis, data curation, Kangxing Du; writing – review & editing, supervision, conceptualization, Guowei Wang; writing – review & editing, writing – original draft, supervision, funding acquisition, conceptualization, Xiaojing Wang; all authors have read and approved the final manuscript.

Conflicts of interest

The authors declare that they have no known competing financial interests or personal relationships that could have appeared to influence the work reported in this paper.

Abbreviations

PROP	Propranolol
CS	Chitosan
PM	Peri-implant mucositis
PI	Peri-implantitis
GBR	Guided bone regeneration
CTG	Connective tissue grafting
β-AR	β-adrenergic receptor
MSCs	Mesenchymal stem cells
NE	Norepinephrine
Hacats	Human immortalized keratinocytes
HGFs	Human gingival fibroblasts
GP	Glycerophosphate
SD	Sprague–Dawley
ECM	Extracellular matrix
BV	Bone volume
TV	Tissue volume
BS	Bone surface
Tb.N	Trabecular number
Tb.Sp	Trabecular separation
Tb.Th	Trabecular thickness
BMC	Bone mineral content

Data availability

The data that support the findings of this study are available from the corresponding author upon reasonable request.

Supplementary information (SI) is available. See DOI: https://doi.org/10.1039/d6ra00103c.

Acknowledgements

This work was supported by project grants from Natural Science Foundation, Shandong, China (Grant ZR2022MH266); Qingdao Demonstration and Guidance Project of Science and Technology to Benefit the People (Grant 23-2-8-smjk-6-nsh); and Open Research Fund of State Key Laboratory of Oral & Maxillofacial Reconstruction and Regeneration (Grant 2024KA04). The schematic illustration materials were supported by Figdraw and Adobe Illustrator. This study was approved by the Ethics Committee of the Affiliated Hospital of Qingdao University (QYFYWZLL30731).

References

1 Y. Zhang, Z. Cheng, Z. Liu, X. Shen, C. Cai, M. Li and Z. Luo, Functionally Tailored Metal–Organic Framework Coatings for Mediating Ti Implant Osseointegration, *Adv. Sci.*, 2023, **10**, e2303958, DOI: 10.1002/advs.202303958.

2 T. Guo, K. Gulati, H. Arora, P. Han, B. Fournier and S. Ivanovski, Orchestrating soft tissue integration at the transmucosal region of titanium implants, *Acta Biomater.*, 2021, **124**, 33–49, DOI: 10.1016/j.actbio.2021.01.001.

3 T. Guo, K. Gulati, H. Arora, P. Han, B. Fournier and S. Ivanovski, Race to invade: Understanding soft tissue integration at the transmucosal region of titanium dental

implants, *Dent. Mater.*, 2021, **37**, 816–831, DOI: 10.1016/j.dental.2021.02.005.

4 R. Zhao, W. Zhao, J. Huang, M. Fang, Y. Dong, J. Chen, Z. Ji and M. Tian, Prevalence and Risk Factors of Peri-Implant Disease: A Retrospective Case-Control Study in Western China, *Int. J. Environ. Res. Publ. Health*, 2022, **19**(19), DOI: 10.3390/ijerph191912667.

5 M. Stefanini, S. Barootchi, M. Sangiorgi, A. Pispero, M. G. Grusovin, L. Mancini, G. Zucchelli and L. Tavelli, Do soft tissue augmentation techniques provide stable and favorable peri-implant conditions in the medium and long term? A systematic review, *Clin. Oral Implants Res.*, 2023, **34**, 28–42, DOI: 10.1111/clr.14150.

6 J. Xu, X. Hu, S. Jiang, Y. Wang, R. Parungao, S. Zheng, Y. Nie, T. Liu and K. Song, The Application of Multi-Walled Carbon Nanotubes in Bone Tissue Repair Hybrid Scaffolds and the Effect on Cell Growth In Vitro, *Polymers*, 2019, **11**(2), DOI: 10.3390/polym11020230.

7 M. Laroche, Y. Degboe, H. Blain, V. Breuil, R. Chapurlat, B. Cortet and B. Sutter, [Effect of drugs for osteoporosis on cardiovascular diseases and effect of cardio vascular drugs on osteoporosis], *Presse Med.*, 2017, **46**, 159–164, DOI: 10.1016/j.lpm.2016.11.005.

8 I. R. Reid, J. Lucas, D. Wattie, A. Horne, M. Bolland, G. D. Gamble, J. S. Davidson and A. B. Grey, Effects of a beta-blocker on bone turnover in normal postmenopausal women: a randomized controlled trial, *J. Clin. Endocrinol. Metab.*, 2005, **90**, 5212–5216, DOI: 10.1210/jc.2005-0573.

9 A. G. Veldhuis-Vlug, M. W. Tanck, E. J. Limonard, E. Endert, A. C. Heijboer, P. Lips, E. Fliers and P. H. Bisschop, The effects of beta-2 adrenergic agonist and antagonist on human bone metabolism: a randomized controlled trial, *Bone*, 2015, **71**, 196–200, DOI: 10.1016/j.bone.2014.10.024.

10 X. Wu, K. Al-Abedalla, H. Eimar, S. Arekunnath Madathil, S. Abi-Nader, N. G. Daniel, B. Nicolau and F. Tamimi, Antihypertensive Medications and the Survival Rate of Osseointegrated Dental Implants: A Cohort Study, *Clin. Implant Dent. Relat. Res.*, 2016, **18**, 1171–1182, DOI: 10.1111/cid.12414.

11 R. Kaur, C. Tchanque-Fossuo, K. West, Y. Hadian, A. Gallegos, D. Yoon, L. Ismailyan, S. Schaefer, S. E. Dahle and R. R. Isseroff, Beta-adrenergic antagonist for the healing of chronic diabetic foot ulcers: study protocol for a prospective, randomized, double-blinded, controlled and parallel-group study, *Trials*, 2020, **21**, 496, DOI: 10.1186/s13063-020-04413-z.

12 S. Rehou, L. de Brito Monteiro, C. Auger, C. M. Knuth, A. Abdullahi, M. Stanojcic and M. G. Jeschke, Propranolol Normalizes Metabolomic Signatures Thereby Improving Outcomes After Burn, *Ann. Surg.*, 2023, **278**, 519–529, DOI: 10.1097/sla.0000000000005973.

13 D. Li, J. Guo, X. H. Li, Y. Liao, M. M. Zhang, L. Shi, Y. Lin and Y. Liu, A case report of an infant after episodes of paroxysmal supraventricular tachycardia with left ventricular thrombosis and cerebral infarction, *Ann. Palliat. Med.*, 2021, **10**, 8322–8327, DOI: 10.21037/apm-20-1797.

14 H. N. Ranasinghe, N. Fernando, S. Handunnetti, P. N. Weeratunga, P. Katulanda, S. Rajapakse, P. Galappatthy and G. R. Constantine, The impact of propranolol on nitric oxide and total antioxidant capacity in patients with resistant hypertension-evidence from the APPROPRIATE trial, *BMC Res. Notes*, 2020, **13**, 228, DOI: 10.1186/s13104-020-05067-5.

15 Z. L. Zhao, C. Liu, Q. Z. Wang, H. W. Wu and J. W. Zheng, Oral atenolol treatment for infantile hemangiomas: clinical analysis of 133 consecutive patients, *Ann. Transl. Med.*, 2021, **9**, 116, DOI: 10.21037/atm-20-5359.

16 Y. Wu, Q. Zhang, B. Zhao and X. Wang, Effect and mechanism of propranolol on promoting osteogenic differentiation and early implant osseointegration, *Int. J. Mol. Med.*, 2021, **48**(4), DOI: 10.3892/ijmm.2021.5024.

17 T. Aghaloo, J. Pi-Anfruns, A. Moshaverinia, D. Sim, T. Grogan and D. Hadaya, The Effects of Systemic Diseases and Medications on Implant Osseointegration: A Systematic Review, *Int. J. Oral Maxillofac. Implants*, 2019, **34**, s35–s49, DOI: 10.11607/jomi.19suppl.g3.

18 Z. Chen, G. Shen, X. Tan, L. Qu, C. Zhang, L. Ma, P. Luo, X. Cao, F. Yang, Y. Liu, Y. Wang and C. Shi, ID1/ID3 mediate the contribution of skin fibroblasts to local nerve regeneration through Itga6 in wound repair, *Stem Cells Transl. Med.*, 2021, **10**, 1637–1649, DOI: 10.1002/sctm.21-0093.

19 W. Chen, H. I. Batawi, J. R. Alava, A. Galor, J. Yuan, C. D. Sarantopoulos, A. L. McClellan, W. J. Feuer, R. C. Levitt and J. Wang, Bulbar conjunctival microvascular responses in dry eye, *Ocul. Surf.*, 2017, **15**, 193–201, DOI: 10.1016/j.jtos.2016.12.002.

20 G. De Caridi, M. Massara, F. Benedetto, P. Tripodi, F. Spinelli, A. David, R. Grande, L. Butrico, R. Serra and S. de Franciscis, Adjuvant spinal cord stimulation improves wound healing of peripheral tissue loss due to steal syndrome of the hand: clinical challenge treating a difficult case, *Int. Wound J.*, 2016, **13**, 72–76, DOI: 10.1111/iwj.12233.

21 A. El Ayadi, A. Prasai, Y. Wang, D. N. Herndon and C. C. Finnerty, β-Adrenergic Receptor Trafficking, Degradation, and Cell Surface Expression Are Altered in Dermal Fibroblasts from Hypertrophic Scars, *J. Invest. Dermatol.*, 2018, **138**, 1645–1655, DOI: 10.1016/j.jid.2018.01.037.

22 N. Jurcak and L. Zheng, Signaling in the microenvironment of pancreatic cancer: Transmitting along the nerve, *Pharmacol. Ther.*, 2019, **200**, 126–134, DOI: 10.1016/j.pharmthera.2019.04.010.

23 A. Filoni, F. Ambrogio, A. De Marco, A. Pacifico and D. Bonamonte, Topical beta-blockers in dermatologic therapy, *Dermatol. Ther.*, 2021, **34**, e15016, DOI: 10.1111/dth.15016.

24 C. E. Pullar, G. S. Le Provost, A. P. O'Leary, S. E. Evans, B. S. Baier and R. R. Isseroff, β2AR antagonists and β2AR gene deletion both promote skin wound repair processes, *J. Invest. Dermatol.*, 2012, **132**, 2076–2084, DOI: 10.1038/jid.2012.108.

25 R. K. Sivamani, C. E. Pullar, C. G. Manabat-Hidalgo, D. M. Rocke, R. C. Carlsen, D. G. Greenhalgh and R. R. Isseroff, Stress-mediated increases in systemic and local epinephrine impair skin wound healing: potential new indication for beta blockers, *PLoS Med.*, 2009, **6**, e12, DOI: 10.1371/journal.pmed.1000012.

26 S. Jia, X. Wang, G. Wang and X. Wang, Mechanism and application of β-adrenoceptor blockers in soft tissue wound healing, *Med. Res. Rev.*, 2024, **44**, 422–452, DOI: 10.1002/med.21984.

27 T. Baltazard, P. Senet, D. Momar, C. Picard, C. Joachim, A. Adas, C. Lok and G. Chaby, Evaluation of timolol maleate gel for management of hard-to-heal chronic venous leg ulcers. Phase II randomised-controlled study, *Ann. Dermatol. Venereol.*, 2021, **148**, 228–232, DOI: 10.1016/j.annder.2020.11.009.

28 G. Dabiri, J. Tiger, R. Goreshi, A. Fischer and S. Iwamoto, Topical timolol may improve overall scar cosmesis in acute surgical wounds, *Cutis*, 2017, **100**, E27–e28.

29 S. Ojeda, E. Blumenthal, P. Stevens, C. R. Andersen, L. Robles, D. N. Herndon and W. J. Meyer, 3rd, The Safety and Efficacy of Propranolol in Reducing the Hypermetabolic Response in the Pediatric Burn Population, *J. Burn Care Res.*, 2018, **39**, 963–969, DOI: 10.1093/jbcr/iry014.

30 N. Rikihisa, H. Takatsuka, T. Suzuki, Y. Shiko, Y. Kawasaki, M. Hanawa, I. Ishii and N. Mitsukawa, Efficacy and Safety of Propranolol Gel for Infantile Hemangioma: A Randomized, Double-Blind Study, *Biol. Pharm. Bull.*, 2022, **45**, 42–50, DOI: 10.1248/bpb.b21-00500.

31 T. Chen, R. Gudipudi, S. A. Nguyen, W. Carroll and C. Clemmens, Should Propranolol Remain the Gold Standard for Treatment of Infantile Hemangioma? A Systematic Review and Meta-Analysis of Propranolol *Versus* Atenolol, *J. Burn Care Res.*, 2023, **132**, 332–340, DOI: 10.1177/00034894221089758.

32 M. P. Tian, A. D. Zhang, Y. X. Yao, X. G. Chen and Y. Liu, Mussel-inspired adhesive and polypeptide-based antibacterial thermo-sensitive hydroxybutyl chitosan hydrogel as BMSCs 3D culture matrix for wound healing, *Carbohydr. Polym.*, 2021, **261**, 117878, DOI: 10.1016/j.carbpol.2021.117878.

33 P. Li, H. Li, X. Shu, M. Wu, J. Liu, T. Hao, H. Cui and L. Zheng, Intra-articular delivery of flurbiprofen sustained release thermogel: improved therapeutic outcome of collagenase II-induced rat knee osteoarthritis, *Drug Deliv.*, 2020, **27**, 1034–1043, DOI: 10.1080/10717544.2020.1787555.

34 V. Akbari, M. Rezazadeh, N. S. Hanaie and F. Hasanzadeh, Preparation and *in vitro* characterization of histidine trimethyl chitosan conjugated nanocomplex incorporated into injectable thermosensitive hydrogels for localized gene delivery, *Biotechnol. Appl. Biochem.*, 2022, **69**, 1047–1057, DOI: 10.1002/bab.2175.

35 S. C. Tao, J. Y. Huang, Y. Gao, Z. X. Li, Z. Y. Wei, H. Dawes and S. C. Guo, Small extracellular vesicles in combination with sleep-related circRNA3503: A targeted therapeutic agent with injectable thermosensitive hydrogel to prevent osteoarthritis, *Bioact. Mater.*, 2021, **6**, 4455–4469, DOI: 10.1016/j.bioactmat.2021.04.031.

36 C. A. Ramírez Barragán, E. R. Macías Balleza, L. García-Uriostegui, J. A. Andrade Ortega, G. Toríz and E. Delgado, Rheological characterization of new thermosensitive hydrogels formed by chitosan, glycerophosphate, and phosphorylated β-cyclodextrin, *Carbohydr. Polym.*, 2018, **201**, 471–481, DOI: 10.1016/j.carbpol.2018.08.076.

37 M. Çalışkan and T. Baran, Design of nanostructured palladium catalyst supported by chitosan/Co(3)O(4) microspheres and investigation of its catalytic behavior against synthesis of benzonitriles, *Int. J. Biol. Macromol.*, 2021, **182**, 722–729, DOI: 10.1016/j.ijbiomac.2021.04.068.

38 K. Pieklarz, G. Galita, M. Tylman, W. Maniukiewicz, E. Kucharska, I. Majsterek and Z. Modrzejewska, Physico-Chemical Properties and Biocompatibility of Thermosensitive Chitosan Lactate and Chitosan Chloride Hydrogels Developed for Tissue Engineering Application, *J. Funct. Biomater.*, 2021, **12**(2), DOI: 10.3390/jfb12020037.

39 M. Rezazadeh, M. Parandeh, V. Akbari, Z. Ebrahimi and A. Taheri, Incorporation of rosuvastatin-loaded chitosan/chondroitin sulfate nanoparticles into a thermosensitive hydrogel for bone tissue engineering: preparation, characterization, and cellular behavior, *Pharm. Dev. Technol.*, 2019, **24**, 357–367, DOI: 10.1080/10837450.2018.1484765.

40 A. Alizadeh, L. Moradi, M. Katebi, J. Ai, M. Azami, B. Moradveisi and S. N. Ostad, Delivery of injectable thermo-sensitive hydrogel releasing nerve growth factor for spinal cord regeneration in rat animal model, *J. Tissue Viability*, 2020, **29**, 359–366, DOI: 10.1016/j.jtv.2020.06.008.

41 S. M. Ahsan, M. Thomas, K. K. Reddy, S. G. Sooraparaju, A. Asthana and I. Bhatnagar, Chitosan as biomaterial in drug delivery and tissue engineering, *Int. J. Biol. Macromol.*, 2018, **110**, 97–109, DOI: 10.1016/j.ijbiomac.2017.08.140.

42 A. Portero, C. Remuñán-López, M. T. Criado and M. J. Alonso, Reacetylated chitosan microspheres for controlled delivery of anti-microbial agents to the gastric mucosa, *J. Microencapsul.*, 2002, **19**, 797–809, DOI: 10.1080/0265204021000022761.

43 O. Felt, P. Buri and R. Gurny, Chitosan: a unique polysaccharide for drug delivery, *Drug Dev. Ind. Pharm.*, 1998, **24**, 979–993, DOI: 10.3109/03639049809089942.

44 I. Kurćubić, U. J. Vajić, S. Cvijić, M. Crevar-Sakač, N. Bogavac-Stanojević, Z. Miloradović, N. Mihajlović-Stanojević, M. Ivanov, D. Karanović, Đ. Jovović and J. Djuriš, Mucoadhesive buccal tablets with propranolol hydrochloride: Formulation development and *in vivo* performances in experimental essential hypertension, *Int. J. Pharm.*, 2021, **610**, 121266, DOI: 10.1016/j.ijpharm.2021.121266.

45 D. L. Melnikova, Z. F. Badrieva, M. A. Kostin, C. Maller, M. Stas, A. Buczek, M. A. Broda, T. Kupka, A. M. Kelterer, P. M. Tolstoy and V. D. Skirda, On Complex Formation between 5-Fluorouracil and β-Cyclodextrin in Solution and in the Solid State: IR Markers and Detection of Short-Lived

Complexes by Diffusion NMR, *Molecules*, 2020, **25**(23), DOI: 10.3390/molecules25235706.

46 J. Liang, J. Li, T. Wang, Y. Liang, X. Zou, G. Zhou and Z. Zhou, [Preparation And Biocompatibility Of *In Situ* Crosslinking Hyaluronic Acid Hydrogel], *Zhongguo Xiufu Chongjian Waike Zazhi*, 2016, **30**, 767–771, DOI: 10.7507/1002-1892.20160156.

47 A. Chenite, C. Chaput, D. Wang, C. Combes, M. D. Buschmann, C. D. Hoemann, J. C. Leroux, B. L. Atkinson, F. Binette and A. Selmani, Novel injectable neutral solutions of chitosan form biodegradable gels in situ, *Biomaterials*, 2000, **21**, 2155–2161, DOI: 10.1016/s0142-9612(00)00116-2.

48 J. Cho, M. C. Heuzey, A. Bégin and P. J. Carreau, Physical gelation of chitosan in the presence of beta-glycerophosphate: the effect of temperature, *Biomacromolecules*, 2005, **6**, 3267–3275, DOI: 10.1021/bm050313s.

49 A. A. Al-Majed, A. H. H. Bakheit, H. A. Abdel Aziz, F. M. Alajmi and H. AlRabiah, *Propranolol, Profiles of Drug Substances, Excipients, and Related Methodology*, 2017, 42, pp. 287–338, DOI: 10.1016/bs.podrm.2017.02.006.

50 Y. Yang, C. Xu, S. Xu, Y. Li, K. Chen, T. Yang, J. Bao, Y. Xu, J. Chen, C. Mao, L. Chen and W. Sun, Injectable hydrogels activated with copper sulfide nanoparticles for enhancing spatiotemporal sterilization and osteogenesis in periodontal therapy, *Biomater. Sci.*, 2025, **13**, 1434–1448, DOI: 10.1039/d3bm02134c.

51 N. Bonnet, C. L. Benhamou, L. Malaval, C. Goncalves, L. Vico, V. Eder, C. Pichon and D. Courteix, Low dose beta-blocker prevents ovariectomy-induced bone loss in rats without affecting heart functions, *J. Cell. Physiol.*, 2008, **217**, 819–827, DOI: 10.1002/jcp.21564.

52 B. Teong, S. M. Kuo, C. H. Chen, Y. K. Chen, Z. J. Cheng and H. H. Huang, Characterization and human osteoblastic proliferation- and differentiation-stimulatory effects of phosphatidylcholine liposomes-encapsulated propranolol hydrochloride, *Biomed. Mater. Eng.*, 2014, **24**, 1875–1887, DOI: 10.3233/bme-140997.

53 M. P. Stapleton, Sir James Black and propranolol. The role of the basic sciences in the history of cardiovascular pharmacology, *Tex. Heart Inst. J.*, 1997, **24**, 336–342.

54 A. V. Srinivasan, Propranolol: A 50-Year Historical Perspective, *Ann. Indian Acad. Neurol.*, 2019, **22**, 21–26, DOI: 10.4103/aian.AIAN_201_18.

55 J. Woroń, M. Siwek and A. Gorostowicz, Adverse effects of interactions between antidepressants and medications used in treatment of cardiovascular disorders, *Psychiatr. Pol.*, 2019, **53**, 977–995, DOI: 10.12740/PP/OnlineFirst/96286.

56 H. M. Zhou, M. L. Zhong, R. H. Wang, C. L. Long, Y. F. Zhang, W. Y. Cui and H. Wang, Synergisms of cardiovascular effects between iptakalim and amlodipine, hydrochlorothiazide or propranolol in anesthetized rats, *Zhongguo Yingyong Shenglixue Zazhi*, 2015, **31**, 532–540.

57 D. M. Bravo-Calderón, A. Assao, N. G. Garcia, C. M. Coutinho-Camillo, M. Roffé, J. N. Germano and D. T. Oliveira, Beta adrenergic receptor activation inhibits oral cancer migration and invasiveness, *Arch. Oral Biol.*, 2020, **118**, 104865, DOI: 10.1016/j.archoralbio.2020.104865.

58 P. Bustamante, D. Miyamoto, A. Goyeneche, P. G. de Alba Graue, E. Jin, T. Tsering, A. B. Dias, M. N. Burnier and J. V. Burnier, Beta-blockers exert potent anti-tumor effects in cutaneous and uveal melanoma, *Cancer Med.*, 2019, **8**, 7265–7277, DOI: 10.1002/cam4.2594.

59 M. A. Tanner, T. P. Thomas, C. A. Maitz and L. A. Grisanti, β2-Adrenergic Receptors Increase Cardiac Fibroblast Proliferation Through the Gαs/ERK1/2-Dependent Secretion of Interleukin-6, *Int. J. Mol. Sci.*, 2020, **21**(22), DOI: 10.3390/ijms21228507.

60 C. S. Wu, D. A. Tsao and H. R. Chang, Beta2-adrenergic receptor agonist inhibits keratinocyte proliferation by mechanisms involving nitric oxide, *Postepy Dermatol Alergol*, 2021, **38**, 396–403, DOI: 10.5114/ada.2020.92918.

61 C. Jeon, K. C. Oh, K. H. Park and H. S. Moon, Effects of ultraviolet treatment and alendronate immersion on osteoblast-like cells and human gingival fibroblasts cultured on titanium surfaces, *Sci. Rep.*, 2019, **9**, 2581, DOI: 10.1038/s41598-019-39355-3.

62 Y. Yang, M. Zheng, Y. Liao, J. Zhou, H. Li and J. Tan, Different behavior of human gingival fibroblasts on surface modified zirconia: A comparison between ultraviolet (UV) light and plasma, *Dent. Mater. J.*, 2019, **38**, 756–763, DOI: 10.4012/dmj.2018-101.

63 K. A. Bielefeld, S. Amini-Nik and B. A. Alman, Cutaneous wound healing: recruiting developmental pathways for regeneration, *Cell. Mol. Life Sci.*, 2013, **70**, 2059–2081, DOI: 10.1007/s00018-012-1152-9.

64 N. G. Fischer and C. Aparicio, Junctional epithelium and hemidesmosomes: Tape and rivets for solving the "percutaneous device dilemma" in dental and other permanent implants, *Bioact. Mater.*, 2022, **18**, 178–198, DOI: 10.1016/j.bioactmat.2022.03.019.

65 Y. Tsubota, C. Yasuda, Y. Kariya, T. Ogawa, T. Hirosaki, H. Mizushima and K. Miyazaki, Regulation of biological activity and matrix assembly of laminin-5 by COOH-terminal, LG4-5 domain of alpha3 chain, *J. Biol. Chem.*, 2005, **280**, 14370–14377, DOI: 10.1074/jbc.M413051200.

66 I. Atsuta, T. Yamaza, M. Yoshinari, T. Goto, M. A. Kido, T. Kagiya, S. Mino, M. Shimono and T. Tanaka, Ultrastructural localization of laminin-5 (gamma2 chain) in the rat peri-implant oral mucosa around a titanium-dental implant by immuno-electron microscopy, *Biomaterials*, 2005, **26**, 6280–6287, DOI: 10.1016/j.biomaterials.2005.03.046.

67 K. C. Bhol, M. J. Dans, R. K. Simmons, C. S. Foster, F. G. Giancotti and A. R. Ahmed, The autoantibodies to alpha 6 beta 4 integrin of patients affected by ocular cicatricial pemphigoid recognize predominantly epitopes within the large cytoplasmic domain of human beta 4, *J. Immunol.*, 2000, **165**, 2824–2829, DOI: 10.4049/jimmunol.165.5.2824.

68 B. Zhao, H. C. van der Mei, G. Subbiahdoss, J. de Vries, M. Rustema-Abbing, R. Kuijer, H. J. Busscher and Y. Ren, Soft tissue integration *versus* early biofilm formation on

different dental implant materials, *Dent. Mater.*, 2014, **30**, 716–727, DOI: 10.1016/j.dental.2014.04.001.

69 I. K. Gipson, S. Spurr-Michaud, A. Tisdale, J. Elwell and M. A. Stepp, Redistribution of the hemidesmosome components alpha 6 beta 4 integrin and bullous pemphigoid antigens during epithelial wound healing, *Exp. Cell Res.*, 1993, **207**, 86–98, DOI: 10.1006/excr.1993.1166.

70 C. R. Bartoli, D. Zhang, J. Kang, S. Hennessy-Strahs, D. Restle, J. Howard, G. Redline, C. Bermudez, P. Atluri and M. A. Acker, Clinical and *In Vitro* Evidence That Subclinical Hemolysis Contributes to LVAD Thrombosis, *Ann. Thorac. Surg.*, 2018, **105**, 807–814, DOI: 10.1016/j.athoracsur.2017.05.060.

71 B. Minkowitz, A. L. Boskey, J. M. Lane, H. S. Pearlman and V. J. Vigorita, Effects of propranolol on bone metabolism in the rat, *J. Orthop. Res.*, 1991, **9**, 869–875, DOI: 10.1002/jor.1100090613.

72 T. Sato, M. Arai, S. Goto and A. Togari, Effects of propranolol on bone metabolism in spontaneously hypertensive rats, *J. Pharmacol. Exp. Ther.*, 2010, **334**, 99–105, DOI: 10.1124/jpet.110.167643.

73 C. Masaoutis and S. Theocharis, The Role of Exosomes in Bone Remodeling: Implications for Bone Physiology and Disease, *Dis. Markers*, 2019, **2019**, 9417914, DOI: 10.1155/2019/9417914.

74 S. K. Wong, K. Y. Chin and S. Ima-Nirwana, The Osteoprotective Effects Of Kaempferol: The Evidence From *In Vivo* And *In Vitro* Studies, *Drug Des., Dev. Ther.*, 2019, **13**, 3497–3514, DOI: 10.2147/dddt.S227738.

75 N. Gürses, A. K. Thorup, J. Reibel, W. G. Carter and P. Holmstrup, Expression of VLA-integrins and their related basement membrane ligands in gingiva from patients of various periodontitis categories, *J. Clin. Periodontol.*, 1999, **26**, 217–224, DOI: 10.1034/j.1600-051x.1999.260404.x.

76 A. K. Rai, K. Janani and R. Rai, Efficacy of Topical Timolol *versus* Saline in Chronic Venous Ulcers: A Randomized Controlled Trial, *J. Cutan. Aesthetic Surg.*, 2020, **13**, 18–23, DOI: 10.4103/jcas.Jcas_13_19.

77 T. Takayama, K. Imamura and S. Yamano, Growth Factor Delivery Using a Collagen Membrane for Bone Tissue Regeneration, *Biomolecules*, 2023, **13**(5), DOI: 10.3390/biom13050809.

78 M. Paczkowska-Walendowska, M. Kulawik, J. Kwiatek, D. Bikiaris and J. Cielecka-Piontek, Chitosan Sponges as Next-Generation Biomaterials for Dental Tissue Engineering and Periodontal Regeneration, *Pharmaceutics*, 2025, **17**(12), DOI: 10.3390/pharmaceutics17121622.

79 A. H. Krauland and M. J. Alonso, Chitosan/cyclodextrin nanoparticles as macromolecular drug delivery system, *Int. J. Pharm.*, 2007, **340**, 134–142, DOI: 10.1016/j.ijpharm.2007.03.005.